Chapter 4

Functional Crosstalk Between α6β4 Nicotinic Acetylcholine Receptors and P2X Receptors

4.1 Introduction

Nicotinic acetylcholine receptors (nAChRs) and P2X receptors are ligand-gated cation channels that mediate cholinergic and purinergic fast synaptic excitation in the nervous system. nAChRs are the member of the Cys-loop receptor family which includes 5-HT_3, $GABA_{A/C}$, and glycine receptors. Cys-loop receptors are composed of five subunits, and each subunit has four transmembrane domains and extracellular *N* and *C*-terminal tails (*1*). There are eight neuronal α (α2–α7, α9, α10) and three neuronal β (β2–β4) nAChR subunits in mammals (*2*). nAChRs are activated by the endogenous neurotransmitter acetylcholine (ACh) as well as nicotine, an alkaloid found in tobacco. P2X receptors belong to a different family of ligand-gated cation channels and are activated by extracellular ATP. The receptors are formed by 3 subunits, composed of one or a combination of the seven (P2X1–P2X7) subunits. Each subunit has two transmembrane domains and intracellular *N* and *C*-terminal tails (*3*).

P2X receptors and nAChRs are structurally different, and as such, they have been assumed to function independently. However, non-independent receptor function was demonstrated between ATP-gated channels and several members of the Cys-loop receptor family (*4–17*). Co-activation of P2X receptors and either nicotinic, serotonin 5-HT_3, or $GABA_{A/C}$ receptors, leads systematically to a cross-inhibitory interaction that translates into non-additivity of the recorded current (*4–17*). Because fast neurotransmitters such as ATP and ACh are co-released in the nervous system (*18–20*), the interactions between their respective receptor channels may play a critical role in shaping synaptic currents.

Dorsal root ganglia (DRG) contain neurons of the peripheral nervous system whose axons convey somatosensory information to the central nervous system (CNS). DRG neurons express a variety of nAChRs with a pharmacology consistent with α7, α3β4*, and α4β2* compositions (where the asterisks denote the possible presence of additional subunits) (*21–25*). Recently, α6β4* was found to be among the subtypes expressed by the DRG (*26*). Meanwhile, P2X2 and P2X3 subunits are heavily expressed in the DRG neurons, and three types of ATP-induced P2X currents were recorded that were consistent with the expression of the homomeric P2X3, homomeric P2X2, and heteromeric P2X2/3 receptors (*27*). The involvement of the ATP-gated receptors in the DRG neurons in nociception is well established.

Very recently, expression genetics and behavioral studies on mutant mice have revealed a negative correlation between expression of α6-nAChR subunit in the DRG neurons and allodynia (sensation of pain in response to a stimulus that

does not normally provoke pain).[1] The result suggests a functional interaction between α6-nAChRs and another pain relevant molecular target in the spinal cord or periphery. We therefore considered the hypothesis that α6β4* nAChRs interact functionally with P2X3 or P2X2/3 receptors, known to be involved in pain.

The present work is aimed to investigate the functional interactions between ATP-activated P2X receptors and α6β4* nAChRs that could potentially reveal a role of α6-nAChR in the anti-allodynic effect. Studies with recombinant nAChRs have identified only two subunit combinations of nAChRs thus far to contain a6 and β4 subunits: α6β4 and α6β4β3 (*28*–*30*). The stoichiometry of the α6β4 composition is currently unknown. β3 was found to assemble with α6 into nicotinic receptor pentamers at several locations in the brain, and only a single β3 subunit is incorporated into nAChR (*31*). β3 does not participate in forming the α:non-α interface that comprises the neuronal ligand-binding site, and other β subunits, either β2 or β4, must be present to form functional nicotinic receptors (*32*). Thus, the stoichiometry of the α6β4β3 composition is likely $(\alpha6)_2(\beta4)_2(\beta3)_1$.

Herein, we studied both the α6β4 and α6β4β3 combinations of nAChRs with three combinations of P2X receptors: homomeric P2X2, homomeric P2X3, and heteromeric P2X2/3 receptors. We report for the first time a functional crosstalk between α6β4* nAChR and P2X receptors in *Xenopus* oocytes. Further studies on the molecular mechanisms reveals two distinct classes of the interaction. The first class is inhibitory and only occurs during the receptor co-

[1] Jeffrey S. Wieskopf, Ardem Patapoutian, and Jeffrey S. Mogil. Personal Communication.

activation by both ACh and ATP. The second class of interaction is pre-organized and constitutive, in which a biophysical property of one channel is modulated by the other. Our finding supports the notion that the α6β4* nAChR may play a role in nociceptive signal transmission in DRG neurons through the cross interaction with P2X receptors.

4.2 Results

4.2.1 Expression of α6β4 and α6β4β3 nAChRs in *Xenopus* oocytes

Most α6-containing nAChRs yield very small agonist-induced currents in heterologous expression experiments, vitiating accurate measurements (*28*–*30*, *33*, *34*). We found that to be true for both α6β4* and α6β2* subtypes with human, rat and mouse α6 subunits. We overcame these problems by using a gain-of-function α6 subunit, α6(L9'S), for α6β4 expression (*35-38*), or a gain-of-function β3 subunit, β3(V13'S), for α6β4β3 expression (*31*, *38*). The wild-type α6β4 produced essentially no current when expressed in oocytes, even when co-expressed with P2X subunits (data not shown). Larger currents were observed from oocytes expressing α6β4β3(V13'S) than α6(L9'S)β4. However, the α6β4β3(V13'S) oocytes were less healthy, frequently displaying less negative resting potentials and larger leak currents when clamped at −60 mV. The leak current could be blocked by mecamylamine, a nicotinic antagonist, suggestive of constitutive activity from the α6β4β3(V13'S) receptor. The observation is

consistent with the spontaneous opening previously reported for the α6β4β3(V13'S) receptor (*38*).

4.2.2 Cross interaction between α6β4* and homomeric P2X2 receptors

While obtaining sufficient α6β4* currents from *Xenopus* oocytes was challenging, the expression of P2X2 receptor was very robust, frequently producing current > 20 μA. When we co-expressed P2X2 with α6(L9'S)β4 or α6β4β3(V13'S) in oocytes, we observed both ACh-evoked current (I_{ACh}) and ATP-evoked current (I_{ATP}) from the same cell. We found only minor (< 2-fold) changes in the EC_{50} values for both ACh and ATP when two types of receptors are co-expressed (Table 4.1). The presence of ATP had only a weak effect on the ACh dose-response relation, and *vice versa*.

As an initial step, we probed the interaction between the two types of receptors by applying a series of saturating doses of agonists in the following sequence: 100 μM ACh, 1 mM ATP, and 100 μM ACh + 1 mM ATP simultaneously. The resulting peak current observed during the co-application of ACh and ATP ($I_{ACh+ATP}$) was compared to the arithmetic sum of the individual ACh- and ATP-induced currents (I_{ACh} and I_{ATP}, respectively) at the same agonist concentrations on the same cell. If the two families of receptors are functionally independent, i.e., if there is no interaction between them, $I_{ACh+ATP}$ is expected to be identical to the predicted sum of I_{ACh} and I_{ATP} of the same cell.

Table 4.1. ACh dose-response results, with or without ATP, from oocytes expressing α6β4* alone or α6β4* with P2X2. ATP dose-response results, with or without ACh, from oocytes expressing P2X2 alone or α6β4* with P2X2

Receptor(s)	Dose-response	Additional Agonist	EC_{50}	Hill Constant	*n*
			μM		
α6(L9′S)β4	ACh		3.3 ± 0.11	1.4 ± 0.05	8
α6β4β3(V13′S)	ACh		1.3 ± 0.06	0.84 ± 0.03	10
P2X2	ATP		24 ± 1.2	1.5 ± 0.10	18
α6(L9′S)β4 + P2X2	ACh		4.3 ± 0.10	1.3 ± 0.03	11
	ACh	32μM ATP	4.5 ± 0.26	1.4 ± 0.09	14
	ACh	100μM ATP	6.0 ± 0.82	1.5 ± 0.23	14
	ATP		22 ± 1.1	1.6 ± 0.11	11
	ATP	100μM ACh	33 ± 3.6	1.3 ± 0.15	11
α6β4β3(V13′S) + P2X2	ACh		1.6 ± 0.09	0.84 ± 0.03	12
	ACh	32μM ATP	2.4 ± 1.1	0.75 ± 0.18	19
	ACh	100μM ATP	1.6 ± 0.45	0.67 ± 0.09	8
	ATP		23 ± 1.7	1.6 ± 0.15	11
	ATP	100μM ACh	24 ± 3.1	1.8 ± 0.35	12

In oocytes co-expressing P2X2−α6(L9′S)β4 or P2X2−α6β4β3(V13′S), we found that when 100 μM ACh and 1mM ATP were applied simultaneously, the total current was approximately 20% less than the sum of the currents elicited by the individual agonist at the same concentrations (Figure 4.1), which is the conventional definition of "cross inhibition." The difference between the predicted current and the observed $I_{ACh+ATP}$ is denoted Δ throughout this chapter. In the case of P2X2–α6(L9′S)β4 oocytes, the mean $I_{ACh+ATP}$ was only slightly larger than the mean I_{ATP} (Figure 4.1). Consequently, the mean Δ was nearly the size of

the average I_{ACh}. When the analogous experiments were performed on cells expressing only α6β4* or only P2X2, we found that ATP did not activate or modulate the α6(L9'S)β4 or α6β4β3(V13'S) nAChRs, and ACh did not activate or modulate the P2X2 receptors (data not shown). The current inhibition suggests that P2X2 and α6β4* receptors were functionally dependent when they were co-expressed, supporting the interaction between the two families of ligand-gated ion channels.

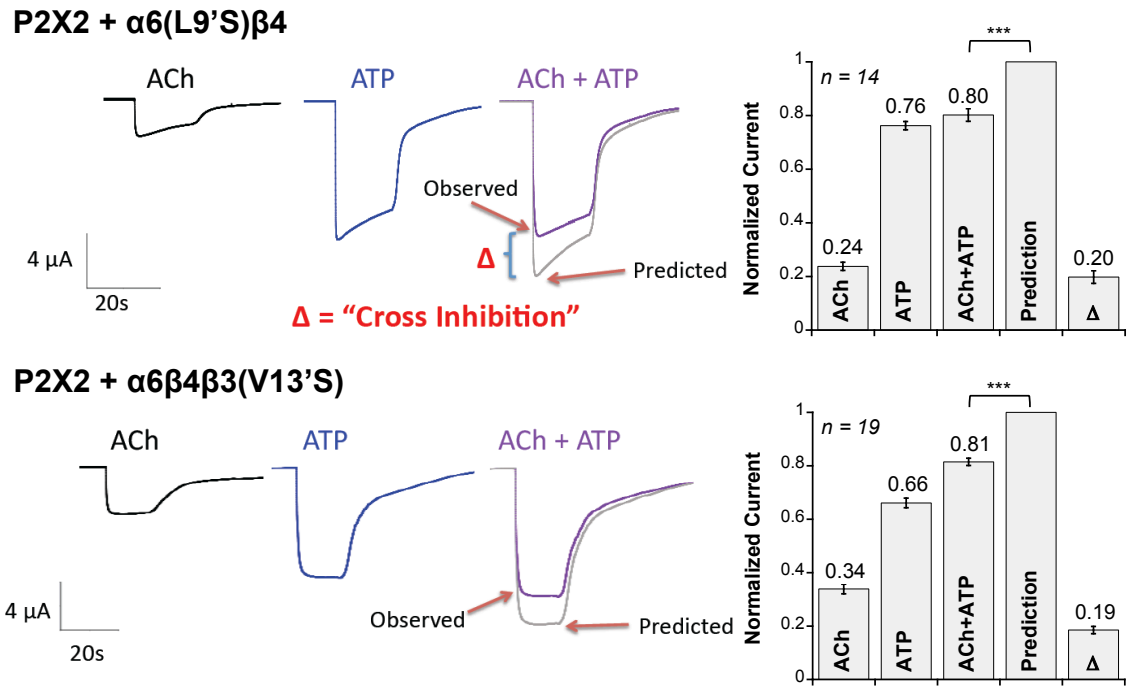

Figure 4.1. Functional interaction between α6β4* nAChRs and P2X2 receptor. Both P2X2–α6(L9'S)β4 oocytes (*top)* and P2X2–α6β4β3(V13'S) oocytes (*bottom)* displayed cross inhibition. Representative current traces from one cell in each case are shown. The predicted waveform is the point-by-point arithmetic sum of the I_{ACh} and I_{ATP} waveforms. Mean normalized currents ± s.e.m. are shown on the right. Δ is the difference between the prediction and the observed $I_{ACh+ATP}$. Currents were normalized to the prediction from the individual cell, and then averaged. ***, $p < 0.0001$.

From the current traces, we noticed that the oocytes expressing both P2X2 and α6(L9′S)β4 consistently produced ATP-evoked current with a sign of receptor desensitization unlike the oocytes expressing P2X2 alone (Figure 4.2) or the α6β4β3(V13′S)–P2X2 oocytes. This observation prompted us to speculate that the desensitized state of P2X2 could be involved in the functional interaction between α6(L9′S)β4 and P2X2 receptors. Further experiments were performed in order to investigate this hypothesis, as discussed later in this chapter.

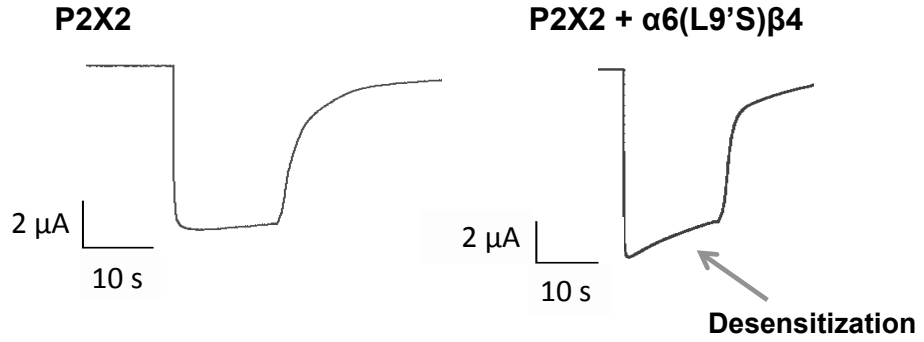

Figure 4.2. Apparent desensitization of ATP-evoked current from P2X2–α6(L9′S)β4. Representative current traces from oocyte expressing P2X2 only (*left*), and oocyte co-expressing α6(L9′S)β4 and P2X2 (*right*)

4.2.3 Cross interaction between α6β4* and homomeric P2X3 receptors

P2X3 receptor desensitizes very rapidly and recovers very slowly from the desensitized state, requiring > 30 minutes for a full recovery (*39*, *40*). Previous work reported that an arginine mutation at the Lys65 residue near the agonist-binding site slightly reduced the rate of desensitization and greatly enhanced the rate of current recovery for the P2X3 receptor expressed in HEK293 cells (*40*).

We mutated this lysine residue to Arg, Gln, Leu, and Ala, and we examined the current traces produced by these mutant receptors expressed in *Xenopus* oocytes. We finally decided to employ the K65A mutation, which produced the most consistent current level (data not shown), as a background mutation for all studies involving the P2X3 receptors. ATP EC_{50} of the P2X3(K65A) receptor was ~ 14 μM, approximately 5-fold higher than the wild-type value, which was reasonable as this residue is located near the ATP-binding site (*41*).

Even in the presence of the K65A mutation, the P2X3 receptors still open and close very rapidly. When ACh and ATP were co-applied to cells expressing α6β4* nAChR and P2X3(K65A), we observed two separate events of inward peak current, presumably arising first from P2X3(K65A) and then α6β4* nAChR openings. This means, most of the P2X3(K65A) receptors opened and desensitized before the opening of the nAChR reached its maximum. The fast desensitization kinetics of the P2X3(K65A) channels did not allow us to perform application of ACh and ATP at the same time, and therefore, the cross interaction protocol described for the P2X2 above could not be used here.

A different protocol was developed to evaluate the cross interaction between the P2X3(K65A) receptors and the α6β4* nAChR (Figure 4.3). ATP-evoked current when ATP was applied alone (I_{ATP}) was compared to the ATP-evoked current when 100 μM ACh was applied before ATP (I_{ATP}*). The difference between I_{ATP} and I_{ATP}* (Δ*) would directly indicate cross interaction between the two receptors.

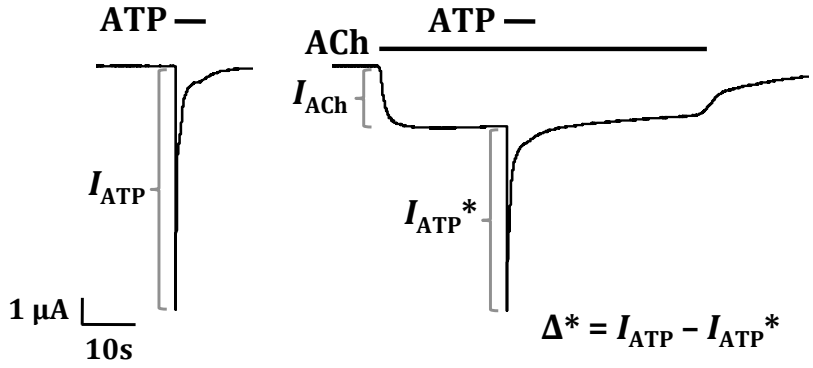

Figure 4.3. The protocol used for probing cross inhibition between α6β4* nAChR and fast-desensitizing P2X receptor. ATP was applied alone *or* after a pre-application of ACh. The resulting ATP-evoked currents from both cases were compared. Δ* is a measurement of cross inhibition.

At 100 μM ACh and 320 μM of ATP, cross inhibition was observed between α6(L9'S)β4 and P2X3(K65A) receptors, in which I_{ATP} was smaller than I_{ATP}* by 23% (Figure 4.4). Control experiments on cells injected with only P2X3(K65A) mRNA confirmed that ACh did not activate or modulate P2X3(K65A) receptors (data not shown). Cross interaction experiments between α6β4β3(V13'S) and P2X3(K65A) receptors were performed at 100 μM of both ACh and ATP. The observed inhibition was smaller than the case of P2X3(K65A)−α6(L9'S)β4, with ~ 17% current reduction from I_{ATP} to I_{ATP}* (Figure 4.4). Both the *p* value and Δ* are smaller than what we typically considered meaningful for establishing a receptor-receptor cross interaction. Thus, we cannot validate the functional interaction between α6β4β3(V13'S) and P2X3(K65A).

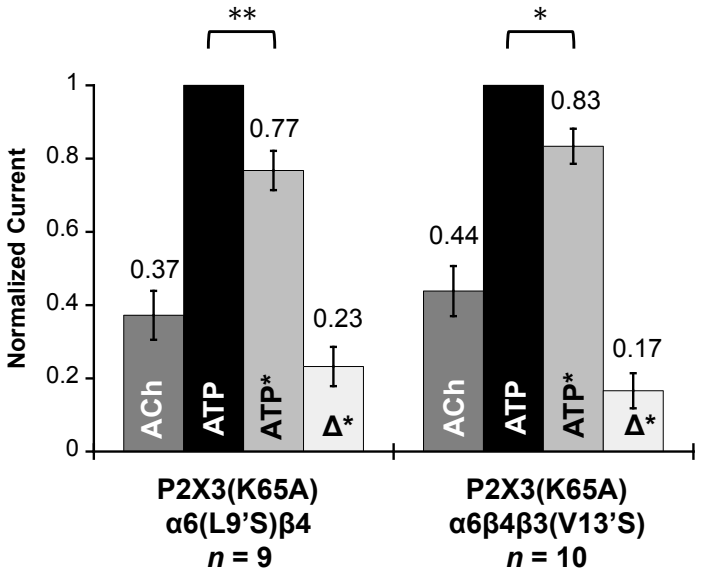

Figure 4.4. Cross inhibition between P2X3(K65A)–α6(L9′S)β4 and P2X3(K65A)–α6β4β3(V13′S). Δ* is the difference between I_{ATP} and I_{ATP}*. Currents were normalized to I_{ATP} from the individual cell, and then averaged. *, $p < 0.01$; **, $p < 0.005$.

In both P2X3(K65A)–α6(L9′S)β4 and P2X3(K65A)–α6β4β3(V13′S) cases, ACh-evoked current when ATP was pre-applied is essentially identical to the ACh-evoked current in the absence of ATP. This means the cross inhibition does not occur when P2X3(K65A) receptor is already desensitized (data not shown).

While co-expression of α6(L9′S)β4 and P2X3(K65A) did not change the ACh EC_{50}, we found that the co-expression caused a rightward shift in the ATP dose-response curve for the P2X3(K65A) receptor. The EC_{50} of the P2X3(K65A) receptor is approximately 3-fold higher, and the response has decreased apparent cooperativity, revealed by a reduced Hill coefficient (Figure 4.5). As a result, responses to ATP in the concentration range 10–100 μM are reduced by approximately half, when normalized to maximal responses. Furthermore, this

shift is independent of ACh (Figure 4.5). Co-expression of α6β4β3(V13'S) and P2X3(K65A) did not meaningfully change the EC_{50} of ACh (1.1 ± 0.10 μM, n = 7) or ATP (7.6 ± 0.33 μM, n = 11) compared to when each individual receptor was expressed alone (ACh EC_{50} 1.3 ± 0.06 μM, n = 10; ATP EC_{50} 13.6 ± 1.3 μM, n = 12).

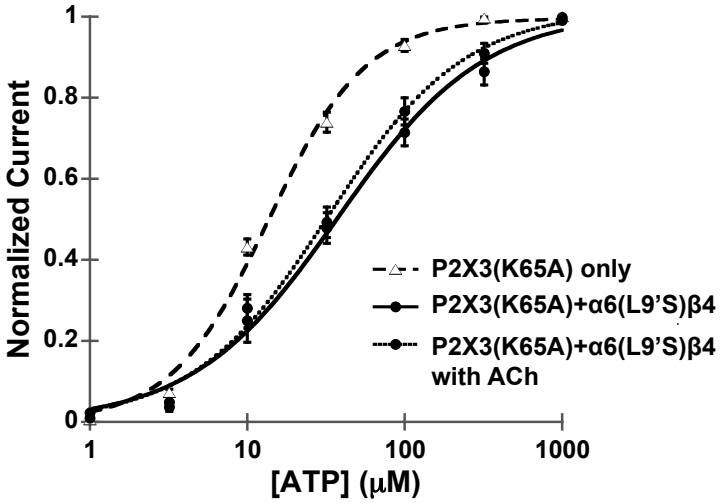

Figure 4.5. ATP dose-response curves for P2X3(K65A) oocytes (EC_{50} 13.6 ± 1.3 μM, Hill constant 1.4 ± 0.16, n = 12), P2X3(K65A)–α6(L9'S)β4 oocytes in the absence of ACh (37.8 ± 6.1 μM, Hill constant 0.94 ± 0.11, n = 14) and in the presence of 100 μM ACh (32.8 ± 5.0 μM, Hill constant 1.0 ± 0.12, n = 11)

Concerning with the accuracy of measuring the fast-desensitizing current, we sought a positive control. Having established that the wild-type P2X2 and the α6(L9'S)β4 receptors interact functionally, we performed parallel experiments on a fast-desensitizing P2X2(T18A) mutant receptor to confirm the validity of our measurement. This alanine mutation at Thr18, which is a phosphorylation site near the *N*-terminus of P2X2, was previously reported to drastically increase the rate of receptor desensitization, producing an apparently similar current trace to

the P2X3 current (*42–44*). Another previous study showed that the fast-desensitizing P2X2(T18A) receptor exhibited the cross-inhibition behavior with α3β4 nAChR similar to the wild-type P2X2 receptor (*41*), suggesting that the mutation did not interfere with the interaction between the P2X receptor and the nAChR.

At saturating concentrations of ATP (1 mM) and ACh (100 μM), we observed cross inhibition between α6(L9'S)β4 and P2X2(T18A), using the same protocol as the P2X3(K65A) experiment. The ATP-evoked current was 28% smaller in the presence of ACh (Figure 4.6A). We also found that the P2X2(T18A) receptor produced an ATP dose-response relation that is similar to the wild-type P2X2 receptor, despite very different desensitizing kinetics (Figure 4.6B). In contrast to what was seen with the P2X3(K65A), co-expressing the α6(L9'S)β4 receptor with the P2X2(T18A) receptor did not affect the ATP EC_{50} (Figure 4.6), which is consistent with the results from the wild-type P2X2 receptor shown in Table 4.1. The data confirm the validity of our protocol for probing fast-desensitizing current, and the rightward shift in the ATP dose-response curve is specific to the interaction between P2X3(K65A) and α6(L9'S)β4.

Overall, the results support the functional interaction between α6(L9'S)β4 and the P2X3(K65A) receptors. At saturated concentration of ATP, reduction in ATP-evoked current was observed in the presence of ACh, indicating a cross inhibition. We did not observe any cross inhibition when P2X3(K65A) was already desensitized. Moreover, oocytes co-expressing α6(L9'S)β4 and P2X3(K65A)

exhibited lower ATP sensitivity in relation to the oocytes expressing P2X3(K65A) alone, independent of α6(L9'S)β4 activation by ACh. In contrast, the interaction between α6β4β3(V13'S) and the P2X3(K65A), if it exists, is much weaker and is *not* firmly established by our data.

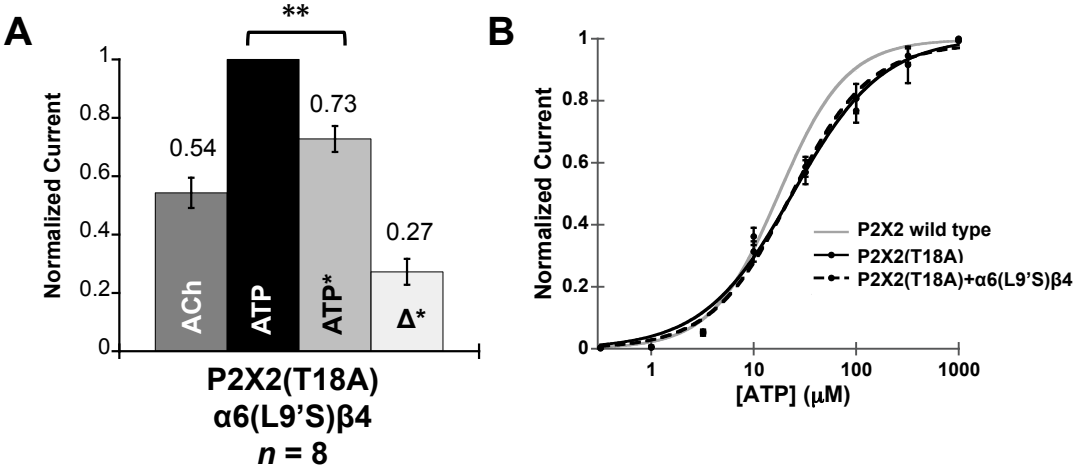

Figure 4.6. Functional interaction between P2X2(T18A) and α6(L9'S)β4. **(A)** Cross inhibition was observed between P2X2(T18A) and α6(L9'S)β4. Δ* is the difference between I_{ATP} and I_{ATP}*. Currents were normalized to I_{ATP} from the individual cell, and then averaged. **, $p < 0.005$. **(B)** ATP dose-response curves for wild-type P2X2 oocytes (EC_{50} 23.9 ± 1.5 μM, Hill constant 1.5 ± 0.10, n = 18), P2X2(T18A) oocytes (24.1 ± 4.8 μM, Hill constant 1.0 ± 0.15, n = 11), and P2X2(T18A)–α6(L9'S)β4 oocytes (22.9 ± 2.7 μM, Hill constant 1.1 ± 0.12, n = 11). Only the curve fit is shown for the wild-type P2X2 oocytes for clarity.

4.2.4. Cross inhibition between α6β4* and heteromeric P2X2/3 receptors

Co-injecting a mixture of P2X2 and P2X3 mRNA into oocytes is known to produce the heteromeric P2X2/3 receptor, along with the homomeric P2X2 and P2X3 receptors (*45*). To exclusively differentiate the P2X2/3 current, we used the

agonist α,β-methylene-ATP (αβmeATP), an ATP analog known to selectively activate the P2X3 and P2X2/3 receptor populations. We employed the wild-type P2X3 subunit, not the K65A mutant, to produce the heteromeric P2X2/3 receptor. The current signal from the homomeric P2X3 receptor was minimized by its intrinsically rapid desensitization. In oocytes co-injected with P2X2 and P2X3 mRNAs, αβmeATP-evoked current traces were distinct from what was seen for the P2X3 oocytes, displaying slower apparent desensitization kinetics. The mRNA injection ratio could be adjusted to favor more heteromeric P2X2/3 receptor expression relative to P2X3 (Figure 4.7C). Nearly pure αβmeATP-evoked current from the P2X2/3 receptors was obtained at the 1:10 P2X2:P2X3 injection ratio by mass; the fast-desensitizing current characteristic of P2X3 was absent (Figure 4.7). Therefore, this was the mRNA ratio used in all studies involving P2X2/3.

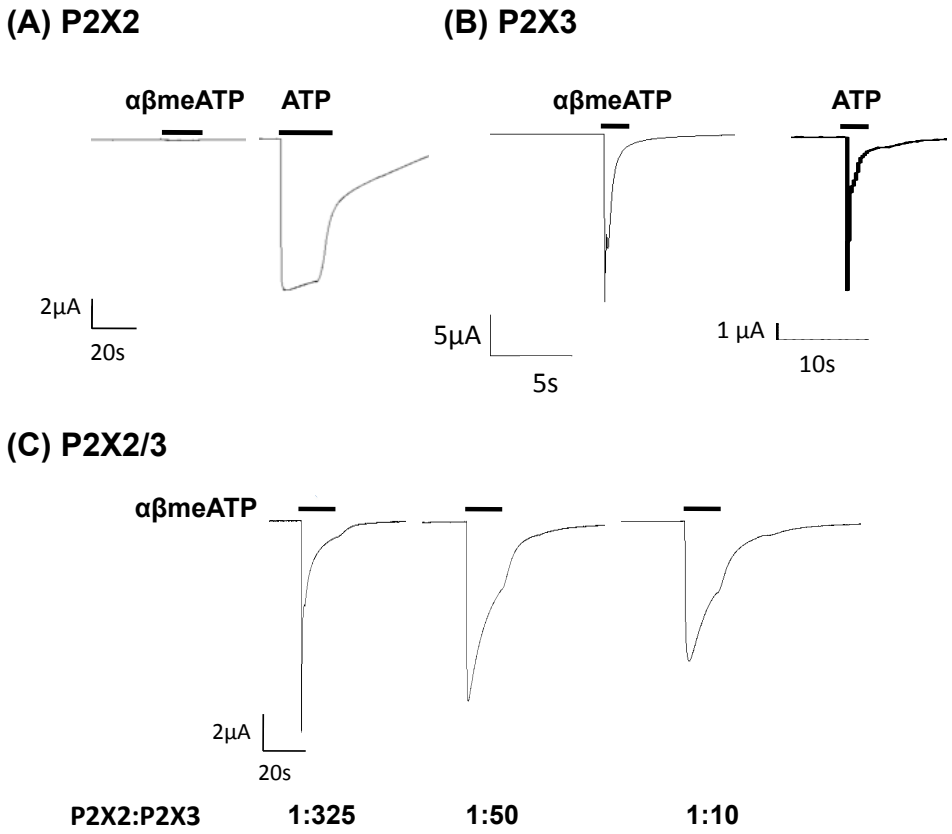

Figure 4.7. Representative current traces as a result of P2X receptor activation by αβmeATP. (A) αβmeATP application did not produce any current in oocytes expressing P2X2 alone. (B) αβmeATP activated the P2X3 receptor, and the current traces show rapid opening and desensitization similar to what was seen when the receptor was activated by ATP. (C) αβmeATP-evoked current traces from oocytes expressed with P2X2 and P2X3 at three different mRNA injection ratios are shown. The heteromeric P2X2/3 receptor desensitizes *less* than the homomeric P2X3 receptor. The P2X2:P2X3 mRNA ratios (by mass) are indicated below the traces.

The heteromeric P2X2/3 receptors produced current traces with a reasonably normal rate of desensitization, permitting us to investigate the cross interaction by simultaneous application of ACh and αβmeATP. Cross-inhibitory behavior was observed when P2X2/3 was co-expressed with α6(L9'S)β4 or α6β4β3(V13'S). In both cases, the current observed when 100 μM αβmeATP and

100 μM ACh were co-applied ($I_{ACh+\alpha\beta_{meATP}}$) was diminished by ≥ 20% compared to the predicted value based on the individual agonist applications (Figure 4.8). Control experiments showed that ACh did not activate or modulate the P2X2/3 receptors in oocytes without α6β4* nAChR. The results support the functional interaction between the α6β4* nAChRs and the heteromeric P2X2/3 receptor.

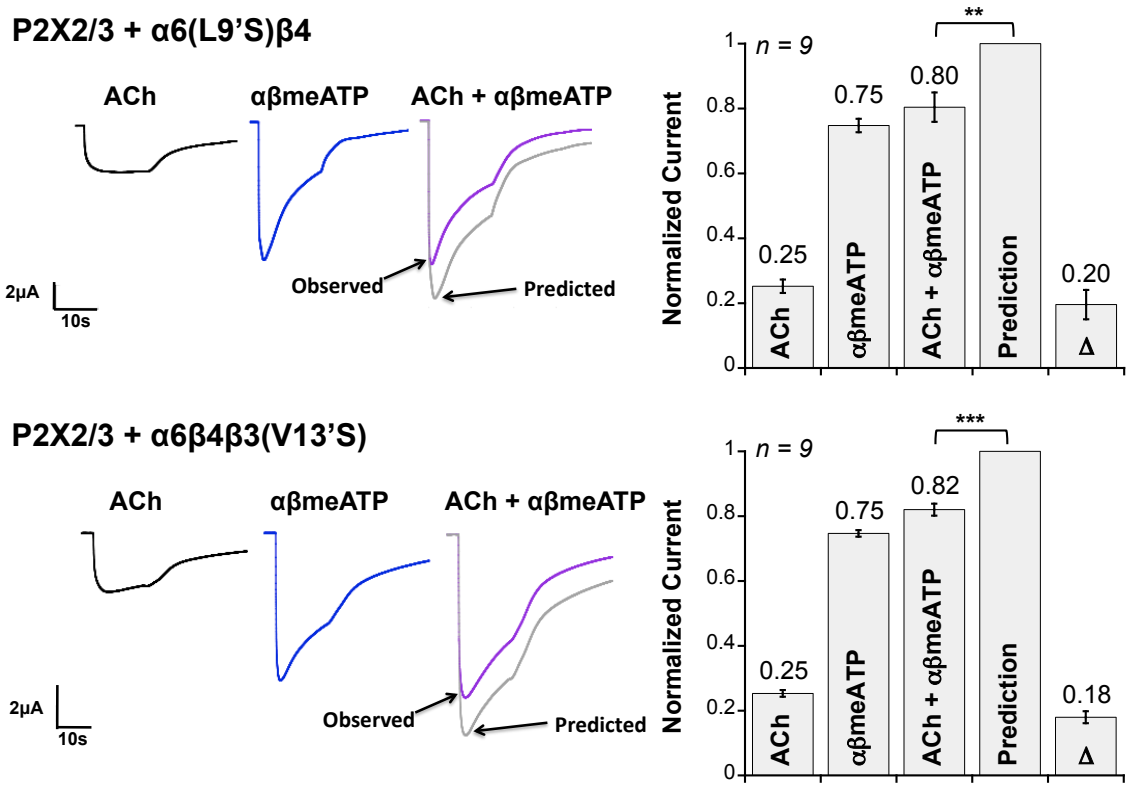

Figure 4.8. Functional interaction between α6β4* nAChRs and P2X2/3 receptor. Both P2X2/3–α6(L9'S)β4 oocytes (*top)* and P2X2/3–α6β4β3(V13'S) oocytes (*bottom)* show cross inhibition. Representative current traces from one cell in each case are shown. The predicted waveform is the point-by-point arithmetic sum of the $I_{\alpha\beta_{meATP}}$ and I_{ACh} waveforms. Mean normalized currents ± s.e.m. are shown on the right. Δ is the difference between the prediction and the observed $I_{ACh+\alpha\beta_{meATP}}$. Currents were normalized to the prediction from the individual cell, and then averaged. **, $p < 0.005$; ***, $p < 0.0001$.

4.2.5 Role of P2X *C*-terminal domains in the cross inhibition

The *C*-terminal domains of P2X2 and P2X3 were previously shown to be crucial for the cross interaction of P2X2 with 5-HT_{3A} receptor, α4β3 nAChR, or $GABA_C$ receptor (*4*, *6*, *7*). To investigate the importance of this domain in the interaction with α6β4* nAChRs, we removed the *C*-terminal tails from both P2X2 and P2X3(K65A) subunits (see materials and methods). The truncated P2X2 and P2X3(K65A) subunits are denoted as P2X2TR and P2X3(K65A)TR, respectively.

Similar to what was seen with the full-length P2X2 receptor, in both α6(L9'S)β4–P2X2TR oocytes and α6β4β3(V13'S)−P2X2TR oocytes, we observed the mean $I_{ACh+ATP}$ values that were ~ 20% smaller than the predicted values (Figure 4.9). These results suggest that the *C*-terminal tail of P2X2 is not required for the functional interaction between the P2X2 receptor and the α6β4* nAChRs.

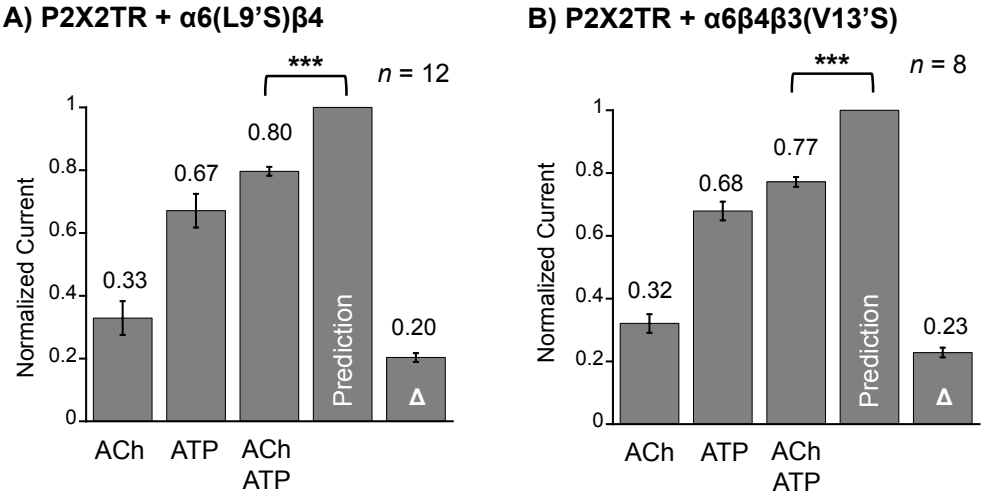

Figure 4.9. Functional interaction between α6β4* nAChRs and P2X2TR receptor. Cross inhibition was observed between the P2X2TR receptor and α6(L9'S)β4 nAChR **(A)**, as well as between the P2X2TR receptor and α6(L9'S)β4 nAChR α6β4β3(V13'S) **(B)**. Currents were normalized to the prediction from the individual cell, and then averaged. Δ is the difference between the prediction and the observed $I_{ACh+ATP}$. ***, $p < 0.0001$.

The P2X3(K65A)TR receptors had comparable ATP EC_{50} to the full-length P2X3(K65A) receptors. Parallel to what was seen with the full-length receptors, co-expression with α6(L9'S)β4 shifted the ATP dose-response curve to the right, increasing the ATP EC_{50} (Figure 4.10). However, we did not observe any cross inhibition between P2X3TR and α6(L9'S)β4 at a saturating ATP concentration (320 μM) (Figure 4.10).

The overall results suggest two distinct modes of cross inhibition between P2X3(K65A) receptors and α6(L9'S)β4: (*i*) a decrease in the maximal I_{ATP} response, which requires the *C*-terminal domain of P2X3 and (*ii*) a decrease in ATP sensitivity, which is independent of the *C*-terminal domain.

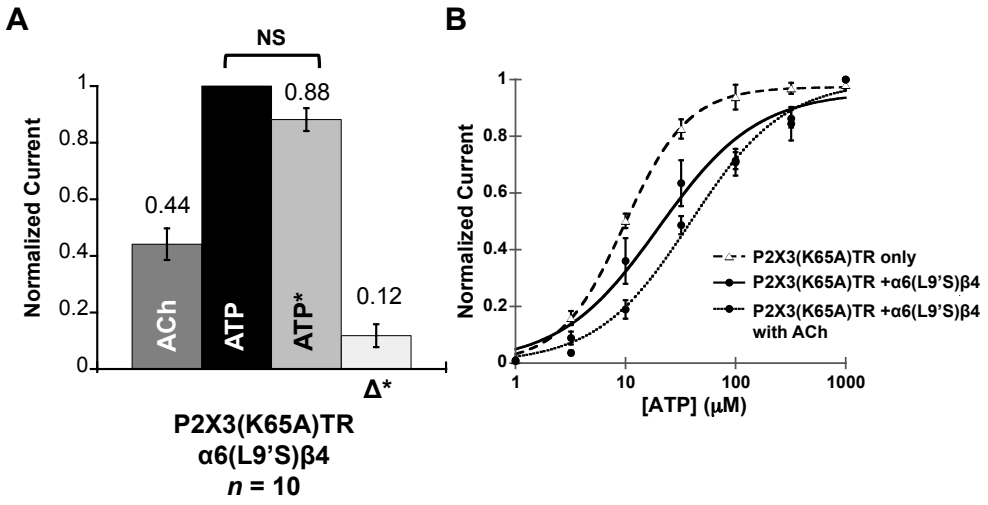

Figure 4.10. Functional interaction between P2X3(K65A)TR and α6(L9'S)β4. **(A)** Cross inhibition was not observed between P2X3(K65A)TR and α6(L9'S)β4. Δ* is the difference between I_{ATP} and I_{ATP*}. Currents were normalized to I_{ATP} from the individual cell, and then averaged. NS, not significant. **(B)** ATP dose-response curves for wild-type P2X3(K65A)TR oocytes (EC_{50} 9.73 ± 0.29 μM, Hill constant 1.5 ± 0.06, n = 6), P2X3(K65A)TR–α6(L9'S)β4 oocytes in an absence of ACh (20.1 ± 5.3 μM, Hill constant 0.97 ± 0.20, n = 7), and P2X3(K65A)TR–α6(L9'S)β4 oocytes in the presence of 100 μM ACh (39.0 ± 6.5 μM, Hill constant 1.0 ± 0.13, n = 8)

4.2.6 Investigation of current occlusion using mecamylamine

The cross-inhibitory behavior observed in oocytes expressing both α6β4* nAChR and P2X receptor during simultaneous application could be a result of an ion channel occlusion that occurred to a subpopulation of the receptors. We sought to use a selective open channel blocker of the nAChR to distinguish between the α6β4* and the P2X ion channel activities during the cross inhibition. (A selective open channel blocker of a P2X receptor has never been reported to our knowledge.) An open channel blocker is considered an uncompetitive antagonist, which only binds to its respective receptor within the open ion pore

following the receptor activation. The conformational change generated by agonist binding that leads to the ion channel opening is *not* affected by the presence of an open channel blocker. Unlike other classes of antagonists, an open channel blocker theoretically should not interfere with the mechanism of cross inhibition. When an α6β4* open channel blocker is applied together with ACh and ATP to an oocyte expressing α6β4* and P2X receptor, one should expect to see the current conducted through the P2X channel pore only. This observed current may or may not be identical to the current evoked by ATP alone on the same cell because of the cross-inhibitory effect when ACh is present. We therefore utilized this strategy to identify the occluded channel pore — either the α6β4* or the P2X.

We decided to experiment with mecamylamine (Mec), a known open channel blocker for several nAChR subtypes, based on the information from the heterologously expressed chimeric nAChRs containing the pore domain of the α6-subunit (*30*, *46*). We found that, in oocytes expressing α6(L9'S)β4 or α6β4β3(V13'S), Mec inhibited ACh-evoked current in a reversible manner, although pre-incubation with the antagonist was required as previously reported with other nAChR subtypes (*30*, *47*). Dose-response experiments were performed, and Mec IC_{50} was determined to be 9.1 ± 0.6 μM for α6(L9'S)β4 and 0.93 ± 0.13 μM for α6β4β3(V13'S). In both cell types, Mec blockade was voltage dependent, showing minimal block at positive potentials (data not shown), which suggests that Mec blocked the α6β4* receptors within the ion pore. In oocytes expressing α6(L9'S)β4 alone or oocytes co-expressing α6(L9'S)β4 and

P2X2, 500 μM Mec blocked > 95% of the ACh-evoked current and did not affect the ATP-evoked current. In oocytes expressing α6β4β3(V13'S) alone or co-expressing α6β4β3(V13'S) and P2X2, similarly, > 95% ACh-evoked current was blocked by 50 μM of Mec, while Mec did not affect the ATP-evoked current. Thus, mecamylamine served as a suitable open channel blocker for the purpose of this experiment. Furthermore, because Mec inhibited the ACh-evoked current nearly completely while leaving the ATP-evoked current unaffected, the data also indicate that the interaction between α6β4* and P2X2 receptors did not involve a cross activation of P2X2 receptor by ACh or a cross activation of α6β4* by ATP.

Co-application of ACh, ATP, and Mec produced an inward current ($I_{ACh+ATP+Mec}$) that was smaller than the current induced by ACh and ATP ($I_{ACh+ATP}$) on the same cells in both α6(L9'S)β4–P2X2 and α6β4β3(V13'S)−P2X2 oocytes. In the case of P2X2–α6(L9'S)β4 oocytes, $I_{ACh+ATP+Mec}$ was significantly smaller than I_{ATP}, and the blocked current, $I_{ACh+ATP+Mec} - I_{ACh+ATP}$ (I_{mec}), was essentially equal to I_{ACh} (Figure 4.11A). Because co-application ACh, ATP, and Mec only produced just the current flowing through P2X2 channels during the cross inhibition, the data suggest that a subpopulation of the P2X2 receptor was inhibited while the α6(L9'S)β4 receptor was fully open during the agonist co-application. In the case of P2X2–α6β4β3(V13'S) oocytes, $I_{ACh+ATP+Mec}$ was essentially the same as I_{ATP} (Figure 4.11B), suggesting that the P2X2 receptor was fully open, in contrast to what was seen with the P2X2–α6(L9'S)β4 oocytes. Moreover, I_{ACh} was essentially

equal to the sum of Δ and I_{Mec} (Figure 4.11), implying that the α6β4β3(V13'S) receptor was inhibited during the cross interaction.

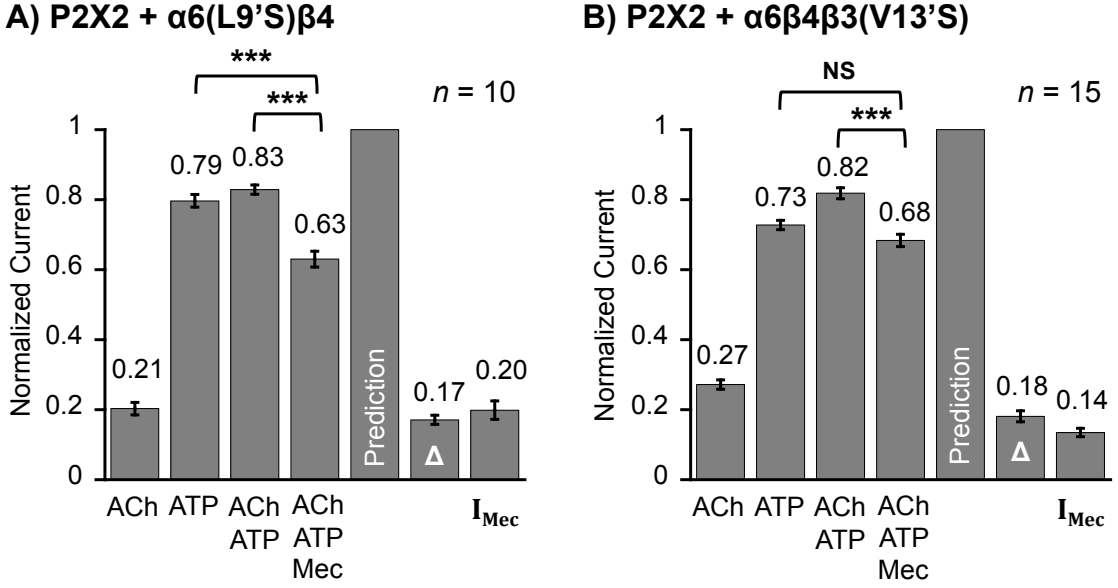

Figure 4.11. Inhibition of $I_{ACh+ATP}$ by mecamylamine in P2X2–α6β4* oocytes. Mean currents elicited by ACh, ATP, ACh+ATP, and ACh+ATP+Mec, respectively, are shown for oocytes expressed with P2X2–α6(L9'S)β4 **(A)** or P2X2–α6β4β3(V13'S) **(B).** Currents were normalized to the prediction from the individual cell, and then averaged. Δ is the difference between the prediction and the observed $I_{ACh+ATP}$. I_{Mec} is the difference between $I_{ACh+ATP+Mec}$ and $I_{ACh+ATP}$. **(A)** $I_{ACh+ATP+Mec} > I_{ATP}$ and $I_{ACh} \approx I_{Mec}$. **(B)** $I_{ACh+ATP+Mec} \approx I_{ATP}$ and $I_{ACh} \approx \Delta + I_{Mec}$. ***, $p <$ 0.0001. NS, not significant

In the case of the P2X2/3 receptor, we found that Mec did not affect $I_{\alpha\beta_{meATP}}$ in the oocytes expressing P2X2/3, regardless of the α6β4* presence. In the oocytes expressing P2X2/3 and α6(L9'S)β4, the current elicited by ACh+αβmeATP+Mec ($I_{ACh+\alpha\beta_{meATP+Mec}}$) was essentially identical to $I_{\alpha\beta_{meATP}}$ (Figure 4.12). The result suggests that the ion pore of the P2X2/3 receptor was fully

open, and thus, the observed inhibition occurred at the α6(L9'S)β4 channel. The oocytes expressing P2X2/3 and α6β4β3(V13'S) showed a slight difference in the amplitudes of $I_{ACh+\alpha\beta meATP+Mec}$ and $I_{\alpha\beta meATP}$, which was not statistically meaningful. Similar to the case of P2X2/3–α6(L9'S)β4, current occlusion did not occur at the P2X2/3 channel pore. Comparison between I_{ACh} and I_{Mec} is not meaningful here due to the mixed I_{ACh} signals arising from the α6β4*–P2X2, α6β4*–P2X3, and α6β4*–P2X2/3 interactions.

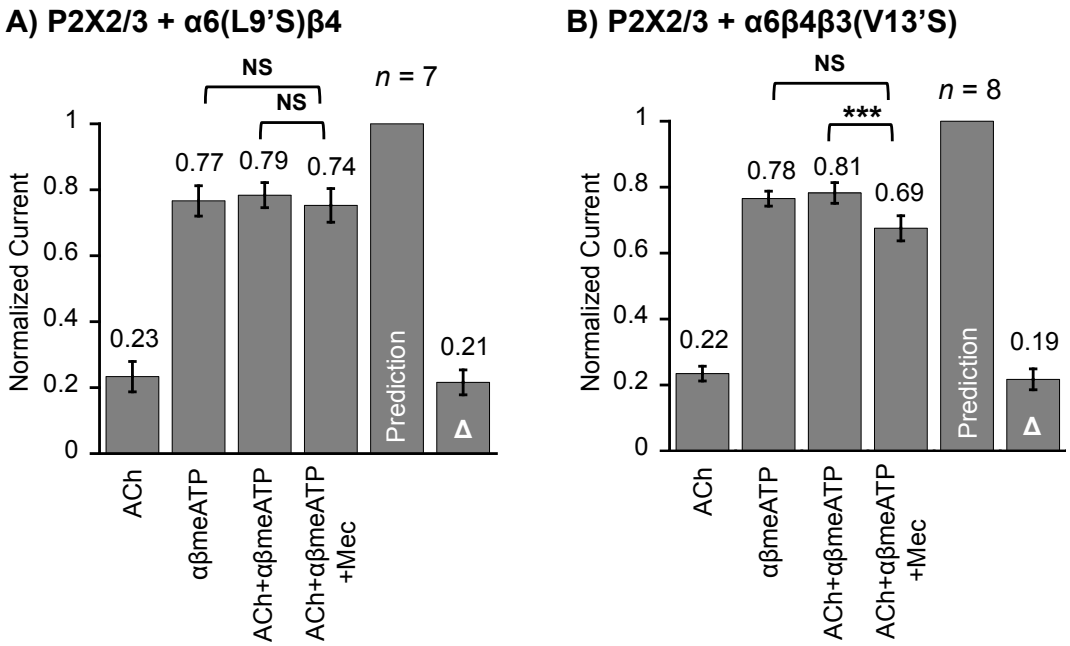

Figure 4.12. Inhibition of $I_{ACh+\alpha\beta meATP}$ by mecamylamine in P2X2/3–α6β4* oocytes. Currents elicited by ACh, αβmeATP, ACh+αβmeATP, and ACh+αβmeATP+Mec are shown for oocytes expressed with P2X2/3–α6(L9'S)β4 **(A)** and P2X2/3–α6β4β3(V13'S) **(B).** Currents were normalized to the prediction from the individual cell, and then averaged. Δ is the difference between the prediction and the observed $I_{ACh+\alpha\beta meATP}$. ***, $p < 0.0001$. NS, not significant

Even though we demonstrated from the mecamylamine block that the α6(L9′S)β4 receptor was fully open during the cross interaction with P2X2 receptor, we could not detect any effect of mecamylamine on the oocytes co-expressing α6(L9′S)β4 and the fast-desensitizing P2X2(T18A) (data not shown). The opening of the P2X2(T18A) receptor was likely too brief for the cross interaction to be probed by this type of experiment. We suspected that the insufficient opening lifetime would be the case for the P2X3 receptor as well, even in the presence of the K65A mutation. Therefore, only the data from the P2X2–α6β4* and P2X2/3–α6β4* oocytes are reported.

4.2.7 Role of P2X2 desensitized state in the cross interaction with α6(L9′S)β4 nAChR

The different ATP current traces between oocytes expressing P2X2 only and P2X2+α6(L9′S)β4 led us to speculate that P2X2 desensitization was involved in the cross inhibition (Figure 4.2). We, therefore, performed more detailed studies on oocytes co-expressing P2X2 and α6(L9′S)β4 for a better understanding of the role of P2X2 desensitization.

On oocytes expressing P2X2 alone and oocytes expressing P2X2–α6(L9′S)β4, we compared the observed current amplitudes as we applied consecutive doses of 1 mM ATP with a 3-minute interval between doses. The P2X2 oocytes showed minimal sign of desensitization upon repeating applications of 1 mM ATP. However, we observed a meaningful reduction in

current size with the P2X2–α6(L9′S)β4 oocytes even though they had never been pre-exposed to an agonist, i.e., the oocytes were *naïve* (Figure 4.13). Similar result was observed when the P2X2–α6(L9′S)β4 oocytes were pre-exposed to ACh. The lost ATP current signal was recoverable over time (data not shown), suggestive of a slow recovery from the desensitized state. However, after a pre-exposure to a mixture of ACh and ATP, repeating ATP doses did not display any reduction in current magnitude (Figure 4.13). This could suggest that the P2X2 receptors had already been desensitized since the application of ACh+ATP. We observed no sign of abnormal ACh desensitization upon repeating application of ACh in oocytes expressing α6(L9′S)β4 alone or co-expressing P2X2 and α6(L9′S)β4 (data not shown). The overall results imply that the P2X2 receptor exhibited a very slow recovery from the desensitized state in the presence of α6(L9′S)β4, regardless of the α6(L9′S)β4 activation by ACh. Thus, the interaction between P2X2 and α6(L9′S)β4 receptor exists prior to the ACh application.

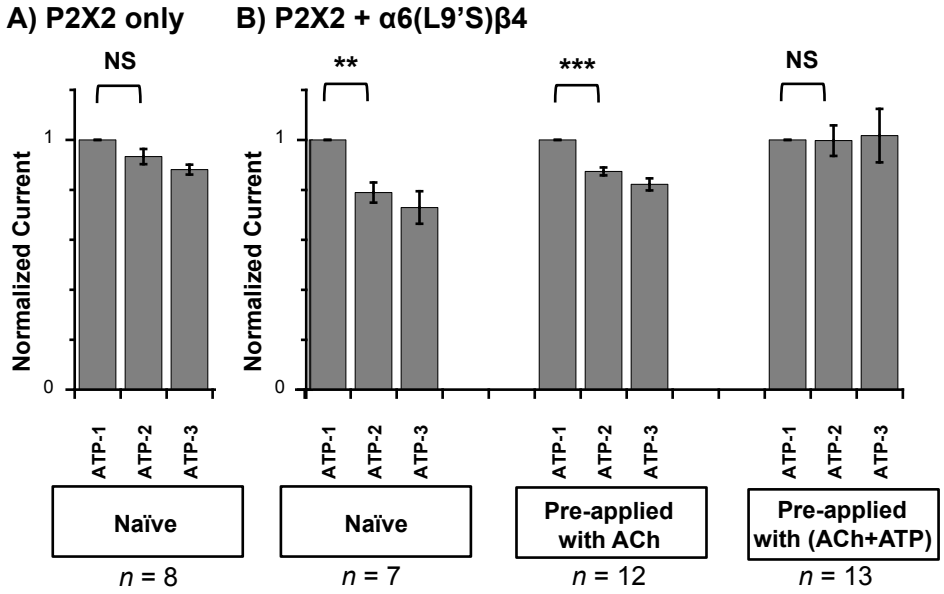

Figure 4.13. The effect of α6(L9'S)β4 on P2X2 desensitized state lifetime. Oocytes were exposed to 3 consecutive doses of 1 mM ATP with a 3-minute interval of wash between doses. Currents were normalized to the current amplitude of the first ATP application from the individual cell, and then averaged. **(A)** Current from P2X2 oocytes display a normal recovery from desensitization. **(B)** Current from naïve P2X2–α6(L9'S)β4 oocytes were only partially recovered after the first ATP dose (*left)*. Incomplete recovery of currents was also observed from oocytes that were exposed to ACh prior to the consecutive doses of ATP (*middle*). However, when oocytes were pre-exposed to an ACh+ATP mixture, no reduction in current amplitudes was observed upon repeating ATP application (*right*). **, $p < 0.005$; ***, $p < 0.0001$. NS, not significant

Next, we asked whether or not cross inhibition would occur between α6(L9'S)β4 and desensitized P2X2 receptors. We tested the P2X2–α6(L9'S)β4 oocytes with a series of agonists in the following order: ACh, four repeating doses of 1mM ATP, ACh+ATP. As expected, ATP-evoked current was smaller upon repeating ATP doses (Figure 4.14, ATP-1 to ATP-4), indicative of a subpopulation of P2X2 being desensitized. Ultimately, no cross inhibition was seen — $I_{ACh+ATP}$ was within error of the predicted sum of the ACh current and the

last ATP current (Figure 4.14). Therefore, the desensitized P2X2 did not functionally interact with the α6(L9′S)β4 nAChR, and the P2X2 desensitization alone could fully explain the cross-inhibitory behavior that we observed.

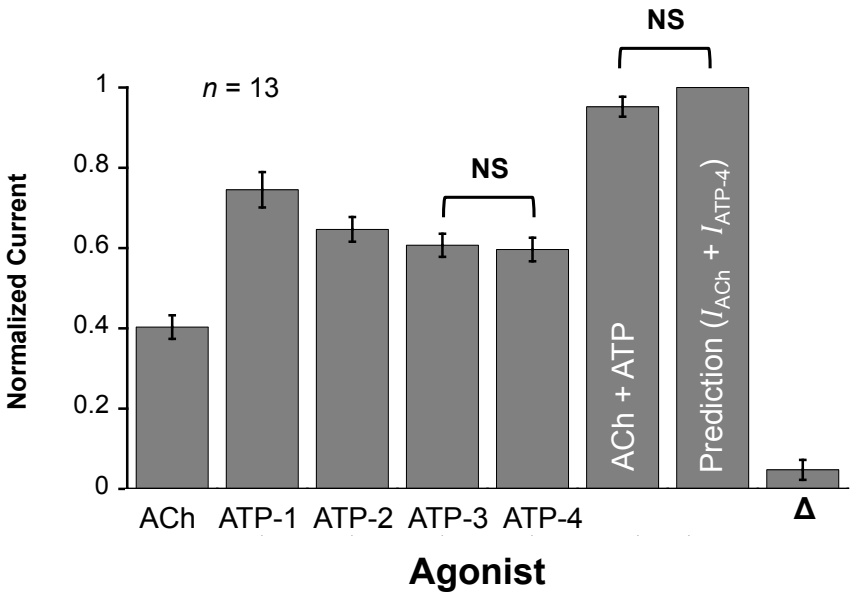

Figure 4.14. Cross inhibition was not observed between desensitized P2X2 and α6(L9′S)β4. P2X2–α6(L9′S)β4 oocytes were exposed to 100 μM ACh, 4 × 1 mM ATP, and (100 μM ACh + 1mM ATP), respectively, with a 3-minute interval of wash between agonist applications. Currents were normalized to the prediction from the individual cell (ACh + ATP-4), and then averaged. Δ is the difference between the prediction and the observed I_{ATP}. NS, not significant

In order to confirm the role of P2X2 desensitization in the functional cross interaction with α6(L9′S)β4, we switched the order of agonist applications in six different combinations. We observed cross inhibition in three out of six cases. In all of the cases that exhibited cross inhibition, ATP was applied before the mixture of ACh and ATP (Figure 4.15). The result is consistent with the notion that a subpopulation of P2X2 was desensitized after an exposure to ATP, causing the apparent cross inhibition.

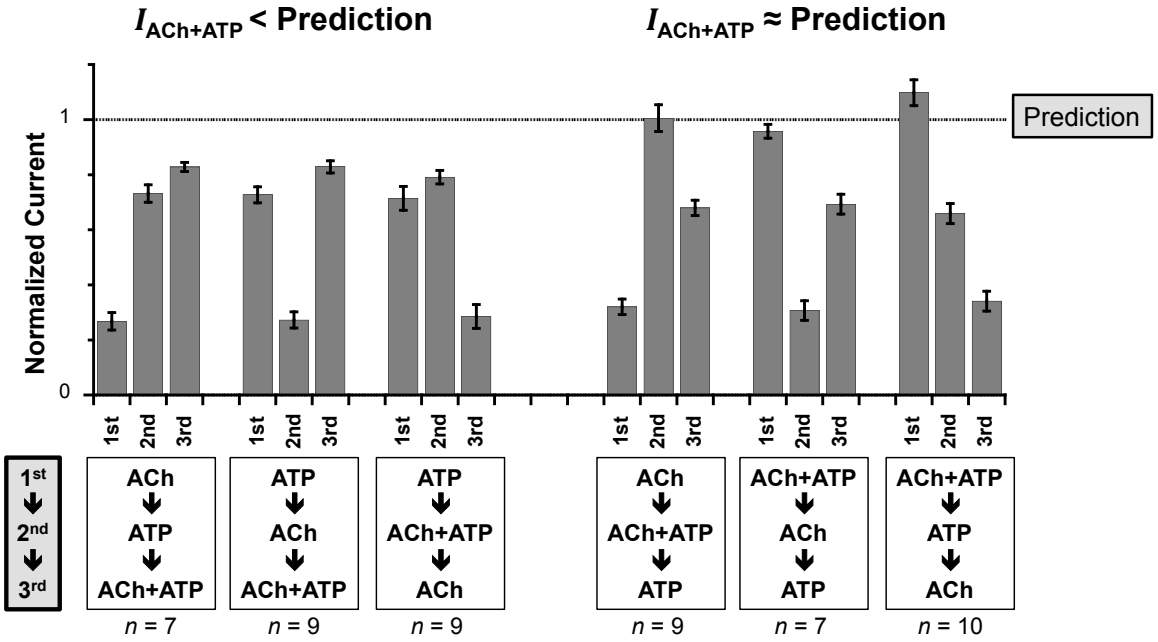

Figure 4.15. Varying sequences of agonist applications produced both non-additive currents (*left*) and additive currents (*right*) from P2X2–α6(L9′S)β4 oocytes. Sequences of agonist applications are indicated at the bottom. There is a 3-minute interval of wash between two agonist applications. Currents were normalized to the prediction from the individual cell, and then averaged.

If the prolonged desensitized state of P2X2 after an exposure to ATP were the sole mechanism underlying the cross inhibition, one would expect the sum of I_{ACh} and I_{ATP} to be smaller than the observed $I_{ACh+ATP}$ in all the cases that ATP was applied *after* the mixture of ACh and ATP. However, we observed current additivity in all these cases — the mean $I_{ACh+ATP}$ was, in fact, comparable to the sum of I_{ACh} and I_{ATP} (Figure 4.15). Considering that the α6(L9′S)β4-*free* P2X2 receptor population contributed to all of the observed I_{ATP} after being exposed to ACh+ATP (Figure 4.13), the additivity means a fraction of current from the α6(L9′S)β4–P2X2 receptor complex was also missing during the ACh+ATP application. Thus, the inhibition occurred instantaneously during the co-

application of ACh+ATP. Consistent with this new insight, we found that repeating application of ACh+ATP mixture to *naïve* oocytes did not produce traces with a substantial decrease in current amplitudes, lacking a sign of receptor desensitization. This could mean either (*i*) there is another different cross-inhibitory mechanism happening while ACh and ATP were co-applied or (*ii*) P2X2 desensitized instantaneously, as soon as the α6(L9'S)β4 was activated by ACh. To distinguish which ion channels were occluded during the co-application of ACh and ATP would be difficult due to the prolonged desensitized state of P2X2 receptor.

In summary, the results in this section suggest that (*i*) cross inhibition between P2X2 and α6(L9'S)β4 receptors was observed as a result of the prolonged desensitization of P2X2 receptor, (*ii*) the desensitized P2X2 receptor can no longer interact with α6(L9'S)β4 receptor, and (*iii*) cross inhibition also occurred while ACh and ATP were co-applied by an unknown mechanism. These observations are unique to the P2X2–α6(L9'S)β4 interacting pair — there is no obvious sign of prolonged desensitized state from the oocytes co-expressing the P2X2–α6β4β3(V13'S), P2X2/3–α6(L9'S)β4, or P2X2/3–α6β4β3(V13'S) combinations.

4.3 Discussion

Several neuronal cell types co-express nicotinic acetylcholine receptors and P2X receptors. Previous experiments from several laboratories show that the functions of these two ligand-gated ion channel subtypes are modulated by each other when they are activated simultaneously by their own neurotransmitters (*4–10*, *12–17*, *48*). Because these functional interactions have been established in several types of neurons as well as heterologous expression systems, the interaction is not a neuron-specific response and it does not require neuron-specific proteins or other molecules. We extended these studies to interactions between α6β4* nAChRs and P2X2, P2X3, or P2X2/3 receptors in *Xenopus* oocytes. All of these receptors are known to co-express in DRG neurons, where the expression of the α6-nAChR subunit is proposed to have a pain-protection effect through the presumed functional connection with the P2X receptors.

We studied functional interactions in six different combinations of P2X (P2X2, P2X3, and P2X2/3) and α6β4* (α6(L9'S)β4 and α6β4β3(V13'S)) receptors in *Xenopus* oocytes. We began our study by applying a series of agonists at their saturating doses. With five of the six combinations, we found functional interactions in the form of cross inhibition between these two classes of ligand-gated receptors. That is, when ACh and ATP were co-applied, the agonist-induced currents were less than the sum of individual currents. This pattern was observed with either type of α6β4* nAChR expressed with P2X2 (Figure 4.1) or with P2X2/3 receptors (Figure 4.8). When α6β4* nAChRs were expressed alone, ATP did not gate or modulate these receptors, and conversely, ACh did not gate

or modulate P2X receptors when they were expressed alone. Cross inhibition was also observed between α6(L9′S)β4 and P2X3(K65A) receptors (Figure 4.4). In this case, the distinctive waveform of the P2X3(K65A) response allows the direct observation that a fraction of current was inhibited when ATP was applied in the presence of ACh in relation to when it was applied alone.

While the expression of P2X receptors is robust in *Xenopus* oocytes, expression of α6-containing nAChRs in heterologous systems is known to be problematic (*28*, *30*, *49*). Even though we successfully expressed both the α6β4 and α6β4β3 subtypes by using a gain-of-function mutation in the pore region, the current produced by α6β4* nAChR was only a few μA, which was not nearly as large as the P2X current. The presumably limited density of the α6β4* nAChRs on the membrane was a concern for the receptor-receptor interaction to occur. Plasma membrane channel density was previously shown to be a determinant of interactions between α3β4 nAChR and P2X2 receptors in *Xenopus* oocytes (*41*). With the difficulty in α6β4* expression, oocytes co-expressed with α6β4* and P2X produced I_{ACh} that was only 20-50% of I_{ATP} in all of our experiments. We intentionally expressed an excess of the P2X receptors with respect to the α6β4* to gain sufficient receptor density for the receptor interaction. However, the substantial difference in the magnitude of I_{ACh} and I_{ATP} complicated the analysis of our cross-inhibition data. In most cases where cross inhibition was observed, the inhibited current was ~ 75–80% of the expected current; the difference between $I_{ACh+ATP}$ and the predicted value (Δ) never exceed ~ 25% of the prediction.

It is worth mentioning that the extent of current reduction (Δ or Δ*) did not accurately represent the degree of the cross inhibition because these values were also dependent on the density of the two receptors being expressed. Because the inhibited current, Δ or Δ*, was presumably constrained by the available number of the α6β4* population on the cell membrane, comparing Δ (or Δ*) to I_{ACh} provides an additional determination for the significance of the receptor interaction. Figure 4.16 shows that, in all the cases that displayed significant current reduction, the magnitude of the reduced current (Δ or Δ*) is greater than 50% of I_{ACh}. The inhibition was particularly substantial in the case of P2X2–α6(L9′S)β4 and P2X2/3–α6(L9′S)β4 pairs, in which the reduced current was 83% and 93% of I_{ACh}, respectively.

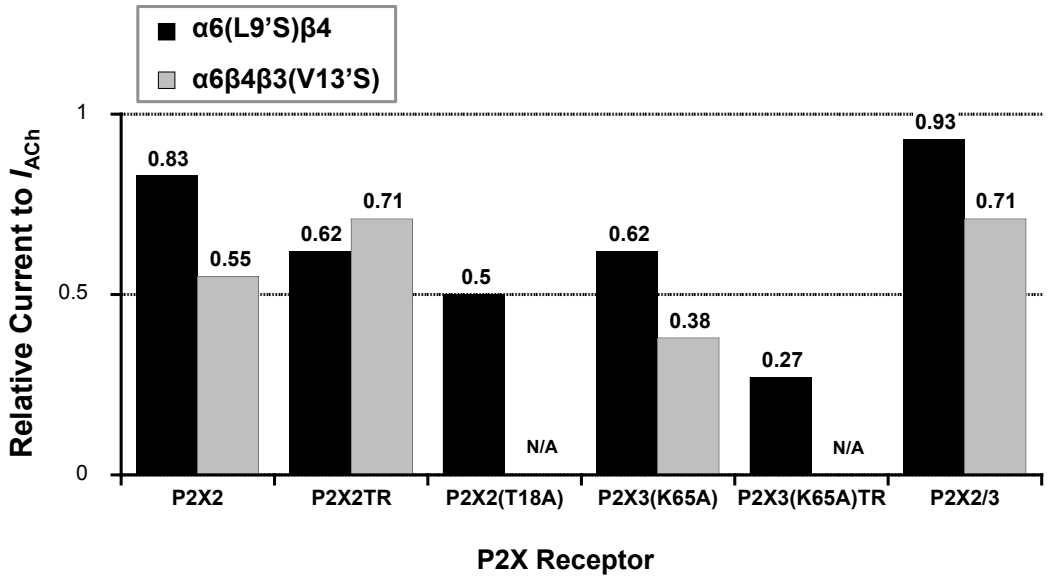

Figure 4.16. Comparison of Δ or Δ* with respect to I_{ACh} across all combinations of receptors. Δ or Δ* was normalized to I_{ACh}. The effect > 0.5 is deemed physiologically significant. N/A, data not available

The crosstalk between the P2X and the Cys-loop families of ligand-gated ion channels has been widely postulated to involve a physical occlusion of the ion channel pores during simultaneous agonist application (*4–7*, *9*, *11*, *13–17*, *50–52*). The proposed models commonly entail a general mechanism of state-dependent "conformational spread" from one receptor to the other. The concept of conformational spread, originally proposed for bacterial chemotaxis receptors, describes the propagation of allosteric states in large multi-protein complexes (*53*). Through this conformational spread, the motion triggered by the gating of one channel type is communicated to the other channels and induces their closure (*4*, *5*, *7*, *8*, *12*). A prerequisite for such a mechanism is the close proximity of receptors.

Physical interactions have been established between P2X2 or P2X3 receptors and α6β4 receptor in Neuro2a cells and cultured mouse cortical neurons by Förster resonance energy transfer (FRET), and moreover, the incorporation of β3 did not alter the binding fraction or the FRET efficiency.[2] Because FRET typically reveals interactions between fluorophores that are less than ~ 80 Å apart, these data imply that the P2X and the α6β4* receptors exist as a macromolecular complex. However, the number of P2X and α6β4* receptors in the protein complex is currently unknown. Previous works also demonstrated physical interactions between α4β2 and P2X2 receptors by FRET (*8*). Additionally, the 5-HT_3 and the $GABA_C$ receptors have been shown to co-precipitate and co-localize with P2X2 receptors by others (*6*, *7*). Evidences for physical interactions eliminate the

[2] Mona Alqazzaz, Christopher R. Richard, and Henry A. Lester, unpublished data

possibility of a major role for second messengers generated by endogenous and electrophysiologically silent metabotropic P2Y in the cross inhibition.

With the evidence for a physical interaction, we assume that *at least* three different populations of receptors existed on the plasma membrane of the oocytes in our experiments: free P2X receptor, free α6β4* receptor, and the α6β4*−P2X complex. We also assume that the free α6β4* population was minimal since the P2X receptors were expressed in excess. It is therefore intriguing that the oocytes expressing P2X2/3 and α6(L9'S)β4, which contained a mixture of P2X2−α6(L9'S)β4, P2X3−α6(L9'S)β4, and P2X2/3−α6(L9'S)β4 populations, exhibited > 90% current inhibition with respect to the ACh-evoked current (Figure 4.16). One possible explanation is that the heteromeric P2X2/3 has a higher affinity for the α6(L9'S)β4 than the homomeric receptors. Alternatively, the presence of multiple P2X receptors in a receptor complex provides another possible explanation; the density of P2X2/3 on the membrane could be so high that every α6(L9'S)β4 receptor had at least one P2X2/3 receptor present in the same complex. However, without a clear view of the cross-inhibitory mechanism of all the receptor combinations on the cells, the underlying cause of the extraordinarily potent cross inhibition between P2X2/3 and α6(L9'S)β4 is still a mystery.

In order to investigate the pore occlusion during the receptor co-activation by ACh and ATP, we used mecamylamine (Mec) for discriminating between the current flowing through α6β4* channel (I_α6) from the current flowing through

the P2X channel (I_P2X). We do *not* make the assumption that I_α6 is necessarily identical to I_{ACh} or I_P2X to I_{ATP} because the two families of proteins are evidently interacting. In oocytes co-expressing P2X2–α6β4*, we found that Mec inhibited > 95% of I_{ACh} without affecting I_{ATP}. This indeed verifies that all ACh-elicited current passed through the α6β4* channel pores exclusively, and the ATP-elicited current only passed through P2X channel pores. The result also suggests that the previous proposal of *channel overlap*, in which ATP activates a subpopulation of the nicotinic receptor channels, is not the case here (*10*). The voltage-dependent nature of the block confirms that Mec binds deep into the membrane and simply occludes channel pore. Hence, the pore blocker is not likely to interfere with the agonist binding, the opening of the pore, or the protein-protein interaction.

Our mecamylamine experiments show that, in three out of four cases, the P2X channel pores were not affected by the cross inhibition. In the case of P2X2–α6β4β3(V13'S), Δ and I_{Mec} also added up to I_{ACh}, providing an internal reference for the occlusion of the α6β4β3(V13'S) channel as both receptors were co-activated. The result from the case of P2X2–α6(L9'S)β4 differs from all other cases that include the β3(V13'S) subunit in the nAChR or the P2X3 subunit, suggesting that the mechanism of the cross inhibition is dependent on both nAChR and P2X receptor subunit compositions. In a previous study, co-activation of P2X2 and various subtypes of $GABA_A$ receptor leads to a functional cross inhibition that was dependent on the $GABA_A$ subunit composition (*5*). By distinguishing the ion conduction through the α6β4* from the P2X channel pores,

the data enable us to identify which receptor was inhibited in all the four combinations that we could test. The experiments, however, only captured a "snapshot" of the cross-inhibition event during the agonist co-application without providing any information regarding the states of the inhibiting or the inhibited receptors at the time of the snapshot.

The results from our investigation of P2X2–α6(L9'S)β4 desensitization clearly supported a role for P2X2 desensitization state in the receptor crosstalk. A subpopulation of the P2X2 receptors desensitized more rapidly and recovered very slowly from the desensitized state — a behavior that was only observed when P2X2 was co-expressed with the α6(L9'S)β4 receptor. The observation was independent of the α6(L9'S)β4 activation by ACh. When we applied a series of agonists in the order of ACh → ATP → ACh+ATP, incomplete recovery of this subpopulation of the receptor after an application of ATP led the apparent current reduction in the subsequent ACh+ATP application, i.e., the cross-inhibition phenomenon. Once desensitized, the P2X2 receptor could no longer functionally interact with the α6(L9'S)β4 receptor (Figure 4.14). We also found that the P2X2 receptors that were pre-exposed to ACh+ATP exhibited a normal recovery from desensitization during the subsequent applications of ATP, implying that all of the α6(L9'S)β4-bound P2X2 receptors had been desensitized during the ACh+ATP exposure (Figure 4.13). Furthermore, when ACh+ATP was applied before ATP, we did not observe any cross inhibition — $I_{ACh+ATP}$ was equal to the sum of the subsequent I_{ACh} and I_{ATP} in all three cases (Figure 4.15). The current additivity shown in Figure 4.15 *cannot* be explained by the absence of

receptor crosstalk. Instead, the apparent additivity of the system suggests that current inhibition had to occur concurrently as ACh+ATP was first applied. Taken together, these data revealed another hidden mode of cross inhibition that was previously obscured by the P2X2 desensitization. This mode of interaction is only detectable during the *first* co-application of ACh and ATP, before the interacting P2X2 population is desensitized. A series of drugs needed to be applied in order to evaluate the results in this type of experiment, and as such the prolonged desensitized state of the interacting P2X2 receptor population limits our ability to probe for the mechanism of the pore occlusion during co-activation of the P2X2–α6(L9′S)β4 complex. Our mecamylamine experiments on the P2X2–α6(L9′S)β4 oocytes were only able to probe the apparent cross inhibition when the interacting P2X2 receptor was already desensitized. The unique characteristic of the P2X2 desensitization was presumably modified simply by being associated with the α6(L9′S)β4 receptor without receptor activation.

Previous works have reported contradicting observations on the cross inhibition during desensitization. Our studies show that, for both P2X2–α6(L9′S)β4 and P2X3(K65A)–α6(L9′S)β4, the functional interaction was lost when the involved P2X receptor was desensitized, which is consistent with a previous study involving cross inhibition between ACh receptor and ATP receptor in rat sympathetic neurons (*10*). In contrast, another work reported that the desensitized P2X2(T18A) receptor could still inhibit α3β4 nAChR (*41*). This result is supported by a more recent study, finding that the α3β4 nAChR can interact with the P2X2, P2X3, and P2X4 receptors during their desensitized state,

although the extent of cross inhibition was not equivalent to that occurring when fully active, non-desensitized receptors were studied (*12*). Nevertheless, the cross-inhibitory mechanism is likely specific to the P2X and nAChR subtypes involved in the interaction.

The case of P2X2–α6(L9′S)β4 indicates that the activation of both interacting receptors is not necessarily required for the functional interaction to take place. Agonist EC_{50} is another convenient probe for receptor function, and a shift in EC_{50} values is suggestive of a gating modulation induced by the crosstalk. In most cases where we could study dose-response relations, we found only minor (< 2-fold) changes in the EC_{50} values for each agonist when we co-expressed these receptors (Table 4.1). An exception is the case with P2X3(K65A)–α6(L9′S)β4, in which the ATP EC_{50} of the P2X3(K65A) receptor was ~ 3-fold higher when the α6(L9′S)β4 receptor was present. These shifts did not depend on the presence of ACh (Figure 4.5). The response also showed a decreased apparent cooperativity, revealed by a reduced Hill coefficient (Figure 4.5). The result implies that cross inhibition also occurred at submaximal concentrations of ATP. The co-expression, however, did not change the EC_{50} for ACh. The presence of α6(L9′S)β4 did not affect the ATP EC_{50} for the fast-desensitizing P2X2(T18A) receptor, while the cross inhibition was still observed between this pair of receptors at the maximal ATP dose. The shift in dose-response relation in the presence of α6(L9′S)β4 is, therefore, a specific P2X3(K65A) character and is not a result of an error in measuring fast-desensitizing current.

The intracellular *C*-terminal domains of P2X2 and P2X3 have been shown to be necessary for the expression of their cross inhibition to some Cys-loop receptors, including α3β4 nAChR, $GABA_A$, $GABA_C$, and 5-HT_3 receptors (*4–7*, *13*). In the case of P2X2−α6β4*, removal of the P2X2 *C*-terminal domain did not affect the cross inhibition at the maximal doses of agonist, and the slow recovery from desensitization was still observed for the P2X2TR receptor co-expressed with α6(L9′S)β4 (data not shown). In the case of P2X3(K65A)–α6(L9′S)β4, we found that the *C*-terminus of P2X3(K65A) is responsible for the current occlusion at the maximal ATP dose but is not required for the rightward shift in the ATP dose-response relation.

The overall results indicate that the P2X−α6β4* interaction is inhibitory. Two distinct mechanisms are suggested to be involved in the functional coupling between these two families of ligand-gated ion channels, highlighted by the results from α6(L9′S)β4 interactions with P2X3(K65A), P2X2(T18A), and P2X3(K65A)TR. The first class takes the form of current occlusion: when both receptors are co-activated by ACh and ATP, the agonist-induced currents are less than the sum of individual currents. This type of mechanism is commonly observed between Cys-loop receptors and P2X receptors.

The interaction likely depends on the physical contact between the two receptors, enabling the activation of one receptor by its agonist to induce a conformational change that results in the pore occlusion of the other ion channel across the protein complex through an allosteric effect. This supports the previous proposal of the conformational spread mechanism. The intracellular *C*-

terminal domains of the P2X receptor possibly play a role in this type of interaction for some P2X–Cys-loop receptor pairs. The second class of P2X–α6β4* interaction is pre-organized. This type of mechanism is constitutive and does not require receptor activation. A change in P2X2 desensitization properties in the presence of α6(L9'S)β4 and a shift in P2X3(K65A) EC_{50} are the examples. The physiology of the ion channels is altered, possibly through physical interaction that possibly does not involve the P2X *C*-terminus. In other words, one receptor may act as a constitutive allosteric modulator of the other. This type of cross inhibition had only been reported for the P2X2–α3β4 nAChR pair, in the forms of constitutive current suppression and the shift in the dose-response relations (*13*). Also supporting this view, competition experiments have shown that expression of a minigene encoding the *C*-terminal domain of P2X2 could disrupt functional interaction but *not* physical interaction between the P2X2 and 5-HT_3 receptors, (*6*) although the constitutive functional interaction was not demonstrated in those experiments.

We have provided evidence supporting functional interactions between α6β4* nAChR and P2X2, P2X3, and P2X2/3 receptors. This could be a mechanism by which the α6-nAChR subunit is involved in the pain pathway. The α6β4* receptor may directly participate in pain sensation through this functional interaction with the P2X receptor. Alternatively, the α6β4* receptor may serve as a means for modulating the activity of P2X receptors through constitutive binding or regulating the interaction of P2X with other receptors. For example, binding of P2X3 receptors to α6β4* in the DRG neurons may compete with the

molecular interaction between the $GABA_A$ receptor and the P2X3 receptor, which has been proposed to play a role in nociceptive signal transmission as well (*4*, *11*). Nonetheless, crosstalk between two ligand-gated ion channels provides a fast and efficient way to adapt neurotransmitter signaling to changing functional needs through a mechanism that appears to be a complex process that is still poorly understood.

4.4 Materials and Methods

Molecular Biology

Rat α6 and mouse β3 nAChRs were in the pGEMhe vector, and rat β4 nAChR was in the pAMV vector. All P2X cDNAs were in the pcDNA3 vector. Site-directed mutagenesis was performed using the Stratagene QuikChange protocol. Truncated P2X2 and P2X3(K65A) subunits were made by engineering a TAA stop codon at the 3′ end of the sequence encoding the residue 373 of P2X2 or residue 385 of P2X3(K65A). Circular cDNA was linearized with NheI (for the pGEMhe vector), NotI (for the pAMV vector), or XhoI (for the pcDNA3 vector). After purification (Qiagen), linearized DNA was used as a template for runoff *in vitro* transcription using T7 mMessage mMachine kit (Ambion). The resulting mRNA was purified (RNAeasy Mini Kit, Qiagen) and quantified by UV-visible spectroscopy.

Expression of α6* nAChR in Xenopus oocytes

Stage V–VI *Xenopus laevis* oocytes were employed. Each oocyte was injected with 50 nL of mRNA solution. When α6β4* nAChR and P2X receptors are co-expressed, equal volume of corresponding mRNA solutions were mixed prior to the oocyte injection. To express the α6β4 combination, we used the hypersensitive α6 subunit containing a serine mutation at the leucine9′ on M2 (residue 279). The mRNA ratio used was 2:5 α6(L9′S):β4 by mass, and we injected 25–50 ng of total mRNA per cell. We used the wild-type α6 and β4 in combination with the hypersensitive β3 containing a serine mutation at the valine13′ on M2 (residue 283) to express the α6β4β3 combination. The wild-type α6β4 produced no detectable current signal, with or without co-injection of the P2X subunits. Cells were injected with a mixture of mRNA at the ratio of 2:2:5 α6:β4:β3(V13′S) at a total mRNA concentration of 5–20 ng per cell. The optimal mRNA concentration of P2X2 was 0.05 ng per cell when expressed alone and 0.1–0.3 ng per cell when co-expressed with α6β4* nAChR. To study P2X3, we used the K65A mutation, which enhanced the rate of recovery from desensitization. We injected 5ng of P2X3(K65A) mRNA per cell when expressed alone and 10–20 ng of mRNA when co-expressed with α6β4* nAChR. P2X2/3 was expressed by co-injection of 1:10 ratio of P2X2:P2X3 mRNA at 15–25 ng of total mRNA. 25–50 ng of mRNA per cell was required to express P2X2(T18A) and the truncated P2X subunits.

After mRNA injection, cells were incubated for 24–72 hours at 18 °C in culture media ($ND96^{+}$ with 5% horse serum).

Electrophysiology

Acetylcholine chloride was purchased from Sigma-Aldrich/RBI and stored as 1M stock solutions in Millipore water. ATP and α,β-methylene-ATP (αβmeATP) were purchased from Tocris Bioscience and were stored as 100 mM stock solutions in Millipore water. Mecamylamine hydrochloride (Mec) was purchased from Sigma and stored as 100 mM stock solutions. All stock solutions were stored at −80°C, and drug dilutions were prepared from the stock solution in calcium-free ND96 buffer within 24 hours prior to the electrophysiological recordings. The pH of all buffers and drug solutions was adjusted to 7.4.

Ion channel function in oocytes was assayed by current recording in two-electrode voltage-clamp mode using the OpusXpress 6000A (Axon Instruments). Up to eight oocytes were simultaneously voltage-clamped at −60 mV. All data were sampled at 125 Hz and filtered at 50 Hz.

For P2X2, α6(L9'S)β4, or α6β4β3(V13'S) dose-response experiments, 1 mL of total agonist solution was applied to cells, and 7-8 concentrations of agonist were used. Mixtures of ATP and ACh were prepared beforehand in cases of agonist co-application. Cells were perfused in calcium-free ND96 solution before agonist application for 30 seconds, followed by a 15-second agonist application and a 2-minute wash in calcium-free ND96 buffer. A similar protocol was used to investigate cross interaction between P2X2 and α6β4*, except that the wash was extended to 3 minutes. 100 μM of ACh and 1 mM of ATP were used in all cross interaction experiments. The order of application was ACh, ATP, and ACh

+ ATP, unless otherwise specified. 50 μM and 500 μM of mecamylamine were used to block α6β4β3(V13'S) and α6(L9'S)β4 receptors, respectively. In all experiments involving mecamylamine, oocytes were incubated with 0.25 mL of mecamylamine (or buffer) for ~ 20 seconds prior to an application of a pre-mixed solution of agonist(s) and mecamylamine (or just agonist(s)). The order of application was ACh, ATP, ACh + ATP, and ACh + ATP + Mec.

To ensure enough channel density, we only analyze data from cells that produced between 5–13 μA of ATP-evoked current (I_{ATP}) and > 1.5 μA of ACh-evoked current (I_{ACh}). Cells displaying larger currents were discarded to avoid the ambiguity associated with error of the measurement as well as other complications arising from extremely high density of receptors such as *pore dilation*, a phenomenon known to occur for P2X2 receptors at high receptor density (*54–58*).

For ATP dose-response experiments on the fast-desensitizing P2X receptors, including P2X3, P2X3(K65A), P2X3TR, and P2X2(T18A) receptors, ATP application was 2-second duration at the total volume of 0.5 mL, and the wash was 3.5 minutes. For ATP dose-response experiments in the presence of ACh, ACh was pre-applied for 15 seconds through pump B (0.6 mL), followed by a 2-second application of a mixture of ATP and ACh (0.5 mL), another 30-second of ACh application through pump B (1.5 mL), and a 164-second wash in calcium-free ND96. Cross interaction between these fast-desensitizing P2X receptors and α6β4* nAChRs was probed in an experiment that involved an alternate application of saturating ATP doses without ACh and with ACh, using the same

protocol as the dose-response experiments, except that the wash time used was 205-second duration. The concentration of ACh was 100 μM in all cross interaction experiments, and the concentrations of ATP were 100 μM for cells expressing P2X3(K65A) and α6β4β3(V13'S), 320 μM for P2X3(K65A) and α6(L9'S)β4, 320 μM for P2X3TR and α6(L9'S)β4, and 1 mM for P2X2(T18A) and α6(L9'S)β4. Peak currents from at least three traces were averaged from the same cell for data analysis. Data from cells displaying < 1.5 μA of I_{ACh}, < 5 μA or > 11 μA of I_{ATP}, or $I_{ACh} > I_{ATP}$ were excluded from all cross-interaction analysis.

To investigate cross interaction between P2X2/3 receptor and α6β4* nAChR, P2X2/3 receptor was activated by 100 μM αβmeATP, and α6β4* nAChR by 100 μM ACh. All agonist applications were 10-second duration at a volume of 0.5 mL, followed by an extra 5-second of incubation with the agonist(s) without fluid aspiration. Then the cells were washed for ~ 5 minutes. The order of application was αβmeATP, ACh, and αβmeATP+ACh, unless specified otherwise. A similar protocol was used for experiments with mecamylamine, and in addition, cells were pre-incubated in 0.25 mL of either buffer or mecamylamine solution prior to the application of the test doses, in the same manner as described above for P2X2–α6β4*. 50 μM and 500 μM of mecamylamine were used to block α6β4β3(V13'S) and α6(L9'S)β4 receptors, respectively. Only data from cells displaying $I_{\alpha\beta_{meATP}}$ between 5-13 μA, $I_{ACh} \geq 1.5$ μA, and $I_{\alpha\beta_{meATP}} > I_{ACh}$ were included in the analysis.

Data Analysis

All dose-response data were normalized to the maximal current (I_{max} = 1) of the same cell and then averaged. EC_{50} and Hill coefficient (n_H) were determined by fitting averaged, normalized dose-response relations to the Hill equation. Dose responses of individual oocytes were also examined and used to determine outliers.

For all cross interaction data involving P2X2 or P2X2/3, including data from the mecamylamine experiments, the predicted current from agonist co-application was calculated from the arithmetic sum of I_{ACh} and I_{ATP} (or $I_{\alpha\beta_{meATP}}$) from the same cell. The actual, observed current upon co-application of the agonists was subtracted from the prediction value of the same cell, and this difference was designated as the Δ. All current data and Δ were normalized to the prediction value of the same cell, and then the normalized data were averaged across at least 7 cells from at least 2 batches of oocytes.

For all cross interaction data involving the fast-desensitizing P2X receptors, including P2X3, P2X3(K65A), P2X3TR, and P2X2(T18A) receptors, averaged ATP-evoked peak current during ACh application (I_{ATP}*) was subtracted from averaged ATP-evoked current in the absence of ACh (I_{ATP}) from the same cell to obtain a Δ*. All current data and Δ* were normalized to (I_{ATP}) and averaged across at least 8 cells from at least 2 batches of oocytes.

All data are presented as mean ± s. e. m. (n = number of cells), with statistical significance assessed by paired Student's t test. A p value of < 0.01 was accepted as indicative of a statistically significant difference.

4.5 References

(1) Unwin, N. Refined structure of the nicotinic acetylcholine receptor at 4Å resolution. *J. Mol. Biol.* **2005**, *346*, 967–989.

(2) Millar, N. S.; Gotti, C. Diversity of vertebrate nicotinic acetylcholine receptors. *Neuropharmacology* **2009**, *56*, 237–246.

(3) Kawate, T.; Michel, J. C.; Birdsong, W. T.; Gouaux, E. Crystal structure of the ATP-gated $P2X_4$ ion channel in the closed state. *Nature* **2009**, *460*, 592–598.

(4) Toulmé, E.; Blais, D.; Léger, C.; Landry, M.; Garret, M.; Séguéla, P.; Boué-Grabot, E. An intracellular motif of $P2X_3$ receptors is required for functional cross-talk with $GABA_A$ receptors in nociceptive DRG neurons. *J. Neurochem.* **2007**, *102*, 1357–1368.

(5) Boué-Grabot, E.; Toulmé, E.; Emerit, M. B.; Garret, M. Subunit-specific coupling between gamma-aminobutyric acid type A and P2X2 receptor channels. *J. Biol. Chem.* **2004**, *279*, 52517–52525.

(6) Boué-Grabot, E.; Emerit, M. B.; Toulmé, E.; Séguéla, P.; Garret, M. Cross-talk and co-trafficking between rho1/GABA receptors and ATP-gated channels. *J. Biol. Chem.* **2004**, *279*, 6967–6975.

(7) Boué-Grabot, E.; Barajas-López, C.; Chakfe, Y.; Blais, D.; Bélanger, D.; Emerit, M. B.; Séguéla, P. Intracellular cross talk and physical interaction between two classes of neurotransmitter-gated channels. *J. Neurosci.* **2003**, *23*, 1246–1253.

(8) Khakh, B. S.; Fisher, J. A.; Nashmi, R.; Bowser, D. N.; Lester, H. A. An angstrom scale interaction between plasma membrane ATP-gated P2X2 and alpha4beta2 nicotinic channels measured with fluorescence resonance energy transfer and total internal reflection fluorescence microscopy. *J. Neurosci.* **2005**, *25*, 6911–6920.

(9) Khakh, B.; Zhou, X.; Sydes, J.; Galligan, J.; Lester, H. State-dependent cross-inhibition between transmitter-gated cation channels. *Nature* **2000**, *406*, 405–410.

(10) Nakazawa, K. ATP-activated current and its interaction with acetylcholine-activated current in rat sympathetic neurons. *J. Neurosci.* **1994**, *14*, 740–750.

(11) Sokolova, E.; Nistri, A.; Giniatullin, R. Negative cross talk between anionic GABAA and cationic P2X ionotropic receptors of rat dorsal root ganglion neurons. *J. Neurosci.* **2001**, *21*, 4958–4968.

(12) Decker, D. A.; Galligan, J. J. Cross-inhibition between nicotinic acetylcholine receptors and P2X receptors in myenteric neurons and HEK-293 cells. *Am. J. Physiol. Gastrointest. Liver Physiol.* **2009**, *296*, G1267–76.

(13) Decker, D. A.; Galligan, J. J. Molecular mechanisms of cross-inhibition between nicotinic acetylcholine receptors and P2X receptors in myenteric neurons and HEK-293 cells. *Neurogastroenterol. Motil.* **2010**, *22*, 901–8, e235.

(14) Karanjia, R.; García-Hernández, L. M.; Miranda-Morales, M.; Somani, N.; Espinosa-Luna, R.; Montaño, L. M.; Barajas-López, C. Cross-inhibitory interactions between $GABA_A$ and P2X channels in myenteric neurones. *Eur. J. Neurosci.* **2006**, *23*, 3259–3268.

(15) Barajas-López, C.; Montaño, L. M.; Espinosa-Luna, R. Inhibitory interactions between 5-HT_3 and P2X channels in submucosal neurons. *Am. J. Physiol. Gastrointest. Liver Physiol.* **2002**, *283*, G1238–48.

(16) Barajas-López, C.; Espinosa-Luna, R.; Zhu, Y. Functional interactions between nicotinic and P2X channels in short-term cultures of guinea-pig submucosal neurons. *J. Physiol. (London)* **1998**, *513 (Pt 3)*, 671–683.

(17) Zhou, X.; Galligan, J. J. Non-additive interaction between nicotinic cholinergic and P2X purine receptors in guinea-pig enteric neurons in culture. *J. Physiol. (London)* **1998**, *513 (Pt 3)*, 685–697.

(18) Galligan, J. J.; Bertrand, P. P. ATP mediates fast synaptic potentials in enteric neurons. *J. Neurosci.* **1994**, *14*, 7563–7571.

(19) Silinsky, E. M.; Redman, R. S. Synchronous release of ATP and neurotransmitter within milliseconds of a motor nerve impulse in the frog. *J. Physiol. (London)* **1996**.

(20) Redman, R. S.; Silinsky, E. M. ATP released together with acetylcholine as the mediator of neuromuscular depression at frog motor nerve endings. *J. Physiol. (London)* **1994**, *477 (Pt 1)*, 117–127.

(21) Genzen, J. R.; Van Cleve, W.; McGehee, D. S. Dorsal root ganglion neurons express multiple nicotinic acetylcholine receptor subtypes. *J. Neurophysiol.* **2001**, *86*, 1773–1782.

(22) Dubé, G. R.; Kohlhaas, K. L.; Rueter, L. E.; Surowy, C. S.; Meyer, M. D.; Briggs, C. A. Loss of functional neuronal nicotinic receptors in dorsal root ganglion neurons in a rat model of neuropathic pain. *Neurosci. Lett.* **2005**, *376*, 29–34.

(23) Fucile, S.; Sucapane, A.; Eusebi, F. Ca2+ permeability of nicotinic acetylcholine receptors from rat dorsal root ganglion neurones. *J. Physiol. (London)* **2005**, *565*, 219–228.

(24) Haberberger, R. V.; Bernardini, N.; Kress, M.; Hartmann, P.; Lips, K. S.; Kummer, W. Nicotinic acetylcholine receptor subtypes in nociceptive dorsal root ganglion neurons of the adult rat. *Auton. Neurosci.* **2004**, *113*, 32–42.

(25) Rau, K. K.; Johnson, R. D.; Cooper, B. Y. Nicotinic AChR in subclassified capsaicin-sensitive and -insensitive nociceptors of the rat DRG. *J. Neurophysiol.* **2005**, *93*, 1358–1371.

(26) Hone, A. J.; Meyer, E. L.; McIntyre, M.; McIntosh, J. M. Nicotinic acetylcholine receptors in dorsal root ganglion neurons include the α6β4* subtype. *FASEB J.* **2012**, *26*, 917–926.

(27) Wirkner, K.; Sperlagh, B.; Illes, P. P2X3 receptor involvement in pain states. *Mol. Neurobiol.* **2007**, *36*, 165–183.

(28) Kuryatov, A.; Olale, F.; Cooper, J.; Choi, C.; Lindstrom, J. Human alpha6 AChR subtypes: subunit composition, assembly, and pharmacological responses. *Neuropharmacology* **2000**, *39*, 2570–2590.

(29) Tumkosit, P.; Kuryatov, A.; Luo, J.; Lindstrom, J. Beta3 subunits promote expression and nicotine-induced up-regulation of human nicotinic alpha6* nicotinic acetylcholine receptors expressed in transfected cell lines. *Mol. Pharmacol.* **2006**, *70*, 1358–1368.

(30) Gerzanich, V.; Kuryatov, A.; Anand, R.; Lindstrom, J. "Orphan" alpha6 nicotinic AChR subunit can form a functional heteromeric acetylcholine receptor. *Mol. Pharmacol.* **1997**, *51*, 320–327.

(31) Drenan, R. M.; Nashmi, R.; Imoukhuede, P.; Just, H.; McKinney, S.; Lester, H. A. Subcellular trafficking, pentameric assembly, and subunit stoichiometry of neuronal nicotinic acetylcholine receptors containing fluorescently labeled alpha6 and beta3 subunits. *Mol. Pharmacol.* **2008**, *73*, 27–41.

(32) Broadbent, S.; Groot-Kormelink, P. J.; Krashia, P. A.; Harkness, P. C.; Millar, N. S.; Beato, M.; Sivilotti, L. G. Incorporation of the beta3 subunit has a dominant-negative effect on the function of recombinant central-type neuronal nicotinic receptors. *Mol. Pharmacol.* **2006**, *70*, 1350–1357.

(33) Xiao, C.; Srinivasan, R.; Drenan, R. M.; Mackey, E. D. W.; McIntosh, J. M.; Lester, H. A. Characterizing functional α6β2 nicotinic acetylcholine receptors in vitro: Mutant β2 subunits improve membrane expression, and fluorescent proteins reveal responsive cells. *Biochem. Pharmacol.* **2011**.

(34) Capelli, A. M.; Castelletti, L.; Chen, Y. H.; Van der Keyl, H.; Pucci, L.; Oliosi, B.; Salvagno, C.; Bertani, B.; Gotti, C.; Powell, A.; Mugnaini, M. Stable expression and functional characterization of a human nicotinic acetylcholine receptor with α6β2 properties: discovery of selective antagonists. *Br. J. Pharmacol.* **2011**, *163*, 313–329.

(35) Drenan, R.; Grady, S.; Whiteaker, P.; McClure-Begley, T.; McKinney, S.; Miwa, J.; Bupp, S.; Heintz, N.; McIntosh, J.; Bencherif, M. In Vivo Activation of Midbrain Dopamine Neurons via Sensitized, High-Affinity α6* Nicotinic Acetylcholine Receptors. *Neuron* **2008**, *60*, 123–136.

(36) Drenan, R.; Grady, S.; Steele, A.; McKinney, S.; Patzlaff, N.; McIntosh, J.; Marks, M.; Miwa, J.; Lester, H. Cholinergic Modulation of Locomotion and Striatal Dopamine Release Is Mediated by α6α4* Nicotinic Acetylcholine Receptors. *J. Neurosci.* **2010**, *30*, 9877.

(37) Cohen, B. N.; Mackey, E. D. W.; Grady, S. R.; McKinney, S.; Patzlaff, N. E.; Wageman, C. R.; McIntosh, J. M.; Marks, M. J.; Lester, H. A.; Drenan, R. M. Nicotinic cholinergic mechanisms causing elevated dopamine release and abnormal locomotor behavior. *Neuroscience* **2012**, *200*, 31–41.

(38) Dash, B.; Bhakta, M.; Chang, Y.; Lukas, R. J. Identification of N-terminal Extracellular Domain Determinants in Nicotinic Acetylcholine Receptor (nAChR) α6 Subunits That Influence Effects of Wild-type or Mutant β3 Subunits on Function of α6β2*- or α6β4*-nAChR. *J. Biol. Chem.* **2011**, *286*, 37976–37989.

(39) Fabbretti, E.; Sokolova, E.; Masten, L.; D'Arco, M.; Fabbro, A.; Nistri, A.; Giniatullin, R. Identification of negative residues in the P2X3 ATP receptor ectodomain as structural determinants for desensitization and the Ca^{2+}-sensing modulatory sites. *J. Biol. Chem.* **2004**, *279*, 53109–53115.

(40) Pratt, E. B.; Brink, T. S.; Bergson, P.; Voigt, M. M.; Cook, S. P. Use-dependent inhibition of P2X3 receptors by nanomolar agonist. *J. Neurosci.* **2005**, *25*, 7359–7365.

(41) Khakh, B. S.; Zhou, X.; Sydes, J.; Galligan, J. J.; Lester, H. A. State-dependent cross-inhibition between transmitter-gated cation channels. *Nature* **2000**, *406*, 405–410.

(42) Boue-Grabot, E. A Protein Kinase C Site Highly Conserved in P2X Subunits Controls the Desensitization Kinetics of P2X2 ATP-gated Channels. *J. Biol. Chem.* **2000**, *275*, 10190–10195.

(43) Brake, A. J.; Wagenbach, M. J.; Julius, D. New structural motif for ligand-gated ion channels defined by an ionotropic ATP receptor. *Nature* **1994**, *371*, 519–523.

(44) Khakh, B. S.; Bao, X. R.; Labarca, C.; Lester, H. A. Neuronal P2X transmitter-gated cation channels change their ion selectivity in seconds. *Nat. Neurosci.* **1999**, *2*, 322–330.

(45) Liu, M.; King, B. F.; Dunn, P. M.; Rong, W.; Townsend-Nicholson, A.; Burnstock, G. Coexpression of $P2X_3$ and $P2X_2$ receptor subunits in varying amounts generates heterogeneous populations of P2X receptors that evoke a spectrum of agonist responses comparable to that seen in sensory neurons. *J. Pharmacol. Exp. Ther.* **2001**, *296*, 1043–1050.

(46) Papke, R.; Dwoskin, L.; Crooks, P.; Zheng, G.; Zhang, Z.; McIntosh, J.; Stokes, C. Extending the analysis of nicotinic receptor antagonists with the study of α6 nicotinic receptor subunit chimeras. *Neuropharmacology* **2008**, *54*, 1189–1200.

(47) Papke, R. L.; Sanberg, P. R.; Shytle, R. D. Analysis of mecamylamine stereoisomers on human nicotinic receptor subtypes. *J. Pharmacol. Exp. Ther.* **2001**, *297*, 646–656.

(48) Sokolova, E.; Nistri, A.; Giniatullin, R. Negative cross talk between anionic $GABA_A$ and cationic P2X ionotropic receptors of rat dorsal root ganglion neurons. *J. Neurosci.* **2001**, *21*, 4958–4968.

(49) Kuryatov, A.; Lindstrom, J. Expression of Functional Human α6 β2α3* Acetylcholine Receptors in *Xenopus laevis* Oocytes Achieved through Subunit Chimeras and Concatamers. *Mol. Pharmacol.* **2011**, *79*, 126–140.

(50) Searl, T. J.; Redman, R. S.; Silinsky, E. M. Mutual occlusion of P2X ATP receptors and nicotinic receptors on sympathetic neurons of the guinea-pig. *J. Physiol. (London)* **1998**, *510 (Pt 3)*, 783–791.

(51) Jiang, L.-H. Identification of Amino Acid Residues Contributing to the ATP-binding Site of a Purinergic P2X Receptor. *J. Biol. Chem.* **2000**, *275*, 34190–34196.

(52) Shakirzyanova, A. V.; Bukharaeva, E. A.; Nikolsky, E. E.; Giniatullin, R. A. Negative cross-talk between presynaptic adenosine and acetylcholine receptors. *Eur. J. Neurosci.* **2006**, *24*, 105–115.

(53) Bray, D.; Duke, T. Conformational spread: the propagation of allosteric states in large multiprotein complexes. *Annu. Rev. Biophys. Biomol. Struct.* **2004**, *33*, 53–73.

(54) Jarvis, M. F.; Khakh, B. S. ATP-gated P2X cation-channels. *Neuropharmacology* **2009**, *56*, 208–215.

(55) Egan, T. M.; Samways, D. S. K.; Li, Z. Biophysics of P2X receptors. *Pflugers Arch. EJP* **2006**, *452*, 501–512.

(56) Fujiwara, Y.; Kubo, Y. Density-dependent changes of the pore properties of the P2X2 receptor channel. *J. Physiol. (London)* **2004**, *558*, 31–43.

(57) Vial, C.; Roberts, J. A.; Evans, R. J. Molecular properties of ATP-gated P2X receptor ion channels. *Trends Pharmacol. Sci.* **2004**, *25*, 487–493.

(58) Eickhorst, A. N.; Berson, A.; Cockayne, D.; Lester, H. A.; Khakh, B. S. Control of $P2X_2$ channel permeability by the cytosolic domain. *J. Gen. Physiol.* **2002**, *120*, 119–131.